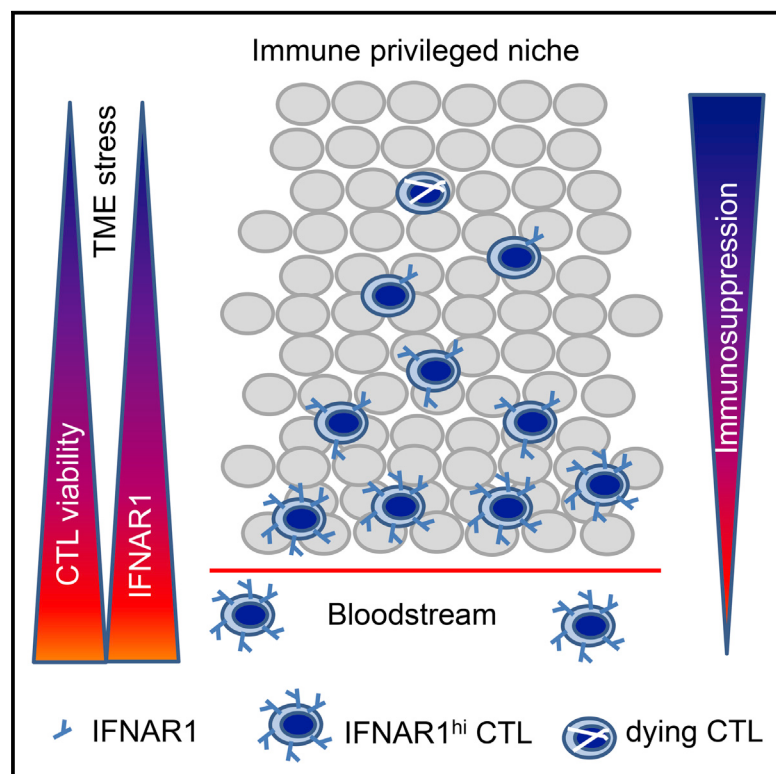


Inactivation of Interferon Receptor Promotes the Establishment of Immune Privileged Tumor Microenvironment

Graphical Abstract



Authors

Kanstantsin V. Katlinski, Jun Gui,
Yuliya V. Katlinskaya, ...,
Constantinos Koumenis, Hallgeir Rui,
Serge Y. Fuchs

Correspondence

syfuchs@upenn.edu

In Brief

Katlinski et al. show reduced type I interferon receptor chain IFNAR1 in colorectal cancer (CRC) stroma, which is important in forming the immune-privileged niche to support CRC development and growth. Stabilization of IFNAR1 improves cytotoxic T lymphocyte survival and suppresses tumor growth.

Highlights

- Colorectal tumors downregulate interferon receptor IFNAR1
- Loss of IFNAR1 promotes generation of immune-privileged niche
- IFNAR1 regulates viability of cytotoxic lymphocytes and efficacy of immunotherapies
- Pharmacologic stabilization of IFNAR1 suppresses tumor growth

Inactivation of Interferon Receptor Promotes the Establishment of Immune Privileged Tumor Microenvironment

Kanstantsin V. Katlinski^{1,7}, Jun Gui^{1,7}, Yuliya V. Katlinskaya¹, Angelica Ortiz¹, Riddhita Chakraborty¹, Sabyasachi Bhattacharya¹, Christopher J. Carbone¹, Daniel P. Beiting², Melanie A. Girondo³, Amy R. Peck³, Ellen Puré¹, Priya Chatterji⁴, Anil K. Rustgi⁴, J. Alan Diehl⁵, Constantinos Koumenis⁶, Hallgeir Rui³, and Serge Y. Fuchs^{1,8,*}

¹Department of Biomedical Sciences, Mari Lowe Center for Comparative Oncology, School of Veterinary Medicine, University of Pennsylvania, Philadelphia, PA 19104, USA

²Department of Pathobiology, School of Veterinary Medicine, University of Pennsylvania, Philadelphia, PA 19104, USA

³Department of Pathology, Medical College of Wisconsin, Milwaukee, WI 53226, USA

⁴Division of Gastroenterology, Department of Medicine, Perelman School of Medicine, University of Pennsylvania, Philadelphia, PA 19104, USA

⁵Department of Biochemistry, Hollings Cancer Center, Medical University of South Carolina, Charleston, SC 29425, USA

⁶Department of Radiation Oncology, Perelman School of Medicine, University of Pennsylvania, Philadelphia, PA 19104, USA

⁷Co-first author

⁸Lead Contact

*Correspondence: syfuchs@upenn.edu

<http://dx.doi.org/10.1016/j.ccr.2017.01.004>

SUMMARY

Refractoriness of solid tumors, including colorectal cancers (CRCs), to immunotherapies is attributed to the immunosuppressive tumor microenvironment that protects malignant cells from cytotoxic T lymphocytes (CTLs). We found that downregulation of the type I interferon receptor chain IFNAR1 occurs in human CRC and mouse models of CRC. Downregulation of IFNAR1 in tumor stroma stimulated CRC development and growth, played a key role in formation of the immune-privileged niche, and predicted poor prognosis in human CRC patients. Genetic stabilization of IFNAR1 improved CTL survival and increased the efficacy of the chimeric antigen receptor T cell transfer and PD-1 inhibition. Likewise, pharmacologic stabilization of IFNAR1 suppressed tumor growth providing the rationale for upregulating IFNAR1 to improve anti-cancer therapies.

INTRODUCTION

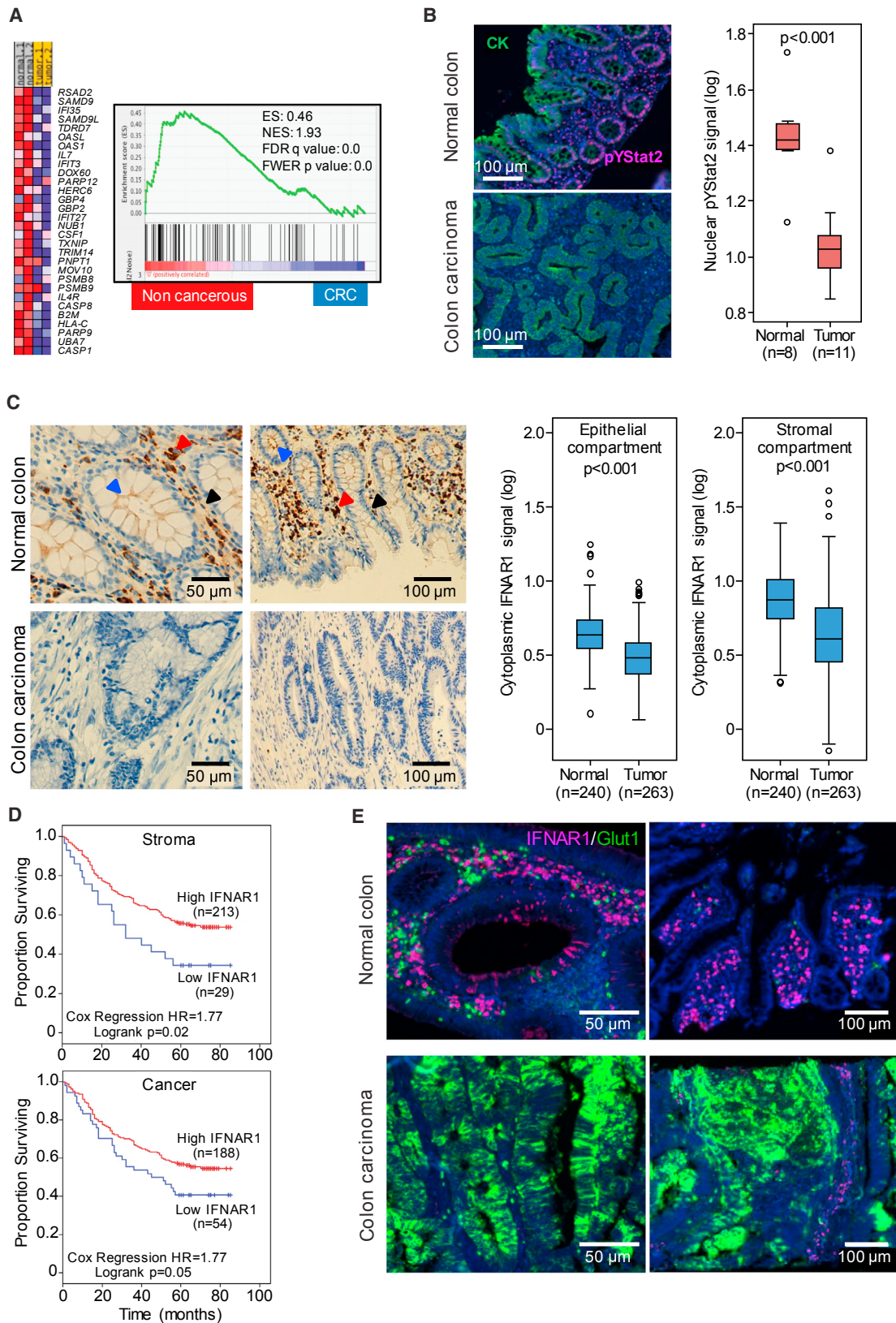
The presence of tumor-specific T cells in the blood of cancer patients, the “Hellström paradox” (Hellström et al., 1968), suggests that, although developing cancers are able to induce a comprehensive immune response, tumors can progress by hindering anti-tumor effector cells (Klemm and Joyce, 2015; Quail and Joyce, 2013). However, recent success in cancer immunotherapy indicates that augmentation of the immune response can improve prognosis. As such, current approaches

to cancer immunotherapy focus on increasing either tumor antigen presentation (via vaccines) or the number of tumor-specific CD8⁺ cytotoxic T lymphocytes (CTLs) (via chimeric antigen receptors [CARs] therapy and other types of adoptive transfer) or enhancing CTL activities (via checkpoint inhibition; reviewed in Rosenberg and Restifo, 2015; Sharma and Allison, 2015).

Regrettably, the majority of patients with solid tumors, including colorectal cancers (CRCs), are refractory to these treatments (Brahmer et al., 2012; Gilham et al., 2012; Topalian

Significance

Understanding the mechanisms by which solid tumors suppress anti-tumor immunity is critical for success of immune therapies. Here we demonstrate that tumor microenvironment factors-induced downregulation of type I interferon receptor IFNAR1 is a central mechanism underlying the ability of the tumor microenvironment to undermine the viability of cytotoxic T cells and to generate intra-tumoral immune-privileged niches devoid of these cells. Means to prevent the loss of IFNAR1 eliminate these niches, inhibit tumor growth, and increase the efficacy of immunotherapies utilizing checkpoint inhibitors or chimeric antigen receptor T cells. These findings delineate a mechanism of localized intra-tumoral immune suppression and prompt the development of IFNAR1-stabilizing agents for use in anti-cancer immune therapies.



(legend on next page)

et al., 2012). Solid tumors evade anti-cancer immune control by establishing immune-privileged niches within the tumor microenvironment (TME). Diverse cellular and acellular (e.g., deficit of oxygen and nutrients) TME elements reduce proliferation, viability, or activity of intra-tumoral CTLs thereby inhibiting their anti-tumor effector function (Fearon, 2014; Joyce and Fearon, 2015; Zhou et al., 2014). Indeed, the apparent exclusion of CTLs from CRC is associated with a poor prognosis (Chiba et al., 2004; Galon et al., 2006; Naito et al., 1998) while, conversely, increased accumulation of CTLs within tumors is associated with a favorable outcome (Talmadge et al., 2007). Delineating the mechanisms that prevent CTL accumulation within the TME remains a major challenge in understanding the immunosuppressive properties of the TME and increase the efficacy of immunotherapies (Joyce and Fearon, 2015).

Studies modeling sarcomas and melanomas in mice lacking the IFNAR1 chain of type I interferon (IFN) receptor suggest that endogenous IFNs contribute to anti-tumor immunity via stimulating specific CD8 α^+ lineage dendritic cells (DCs) to cross-present antigen to CTLs (Diamond et al., 2011; Fuertes et al., 2011; Hildner et al., 2008). IFNs also provide a “third signal” to stimulate the clonal expansion of CD8 $+$ T cells (Aichele et al., 2006; Curtsinger et al., 2005; Hervas-Stubbs et al., 2010) and increase the viability of activated anti-viral CD8 $+$ T lymphocytes (Crouse et al., 2014; Kolumam et al., 2005; Wang et al., 2012; Xu et al., 2014) and tumor-specific CTLs (Hiroishi et al., 2000). These reports are consistent with the long-known anti-tumorigenic effects of IFN (Platanias, 2005; Trinchieri, 2010; Zitvogel et al., 2015). Nevertheless, given that tumorigenesis readily proceeds in IFNAR1-competent mice and humans, it is apparent that cancers manage to overcome the effects of endogenous IFN through a poorly understood mechanism.

Cell surface IFNAR1 levels are critical for all IFN effects (Fuchs, 2013; Uze et al., 2007). These levels are controlled by IFNAR1 ubiquitination and degradation facilitated by the SCF- β Tcrp E3 ligase, which binds to IFNAR1 phosphorylated on Ser535 (Ser526) in mouse IFNAR1; (Kumar et al., 2003). Phosphorylation of these serine residues can be triggered in vitro by stimuli characteristic for the TME such as unfolded protein response (Liu et al., 2009), oxygen or nutrient deficit (Bhattacharya et al., 2013), vascular endothelial growth factor (Zheng et al., 2011), and inflammatory cytokines (Huangfu et al., 2012). Here we aimed to characterize the status of IFNAR1 and IFN signaling in CRC tumors and to determine the importance of IFNAR1 downregulation in establishing the intra-tumoral immune-privileged niche.

RESULTS

IFNAR1 Levels and Signaling Are Reduced in the TME

Global expression profiling within hypoxic areas of transplanted tumors revealed a decrease in expression of the immune response genes (Marotta et al., 2011). We also noted a suppression of the IFN-signaling signature in hypoxic tumor areas characterized by TME stress (Figures S1A and S1B). Importantly, mining of datasets from patients with CRC (Rohr et al., 2013) revealed a decrease in IFN-induced gene expression in tumors compared with benign colorectal tissues from the same patients (Figure 1A). In addition, compared with normal colorectal tissues, tumors exhibited markedly decreased levels of nuclear phosphorylated STAT2 (Figure 1B), which is a downstream effector of IFN signaling (Platanias, 2005). These results suggest that IFN signaling is inhibited in human CRC tumors.

TME-associated stress stimuli such as nutrient/oxygen deficit can cause a loss of IFNAR1 protein in vitro (Bhattacharya et al., 2013). Although comparable IFNAR1 mRNA expression was reported in CRC and normal colorectal tissues (Rohr et al., 2013), we noted dramatic differences in IFNAR1 protein levels. IFNAR1 was detected in all normal human colon cell types including epithelial cells (especially at their apical surface), stromal fibroblasts, and infiltrating immune cells. However, all cell types within human colorectal adenocarcinomas exhibited partial or complete loss of IFNAR1 (Figures 1C and S1C). For these samples, IFNAR1 levels in the cancer cell compartment and in the stromal compartment positively correlated ($r = 0.700$, $p < 0.001$; $n = 263$). Importantly, downregulation of IFNAR1 in either stromal or cancer cell compartments of human CRC tumors were associated with poor prognosis (Figure 1D). Furthermore, whereas many cells expressed high levels of IFNAR1 in normal human colon, those few IFNAR1-positive cells found in colon carcinomas were spatially segregated from the tumor areas, which were positive for GLUT1, a marker of TME stress (Figures 1E and S1D). These data collectively suggest that TME conditions in human CRC prompt IFNAR1 downregulation and suppress IFN signaling.

Downregulation of IFNAR1 in the Stromal Compartment Stimulates Colorectal Tumorigenesis

Guided by these data in human patients, we sought to determine the role of partial loss of IFNAR1 using murine CRC models. Notably, downregulation of IFNAR1 protein observed in human CRC (Figure 1C) was faithfully recapitulated in the mouse model of inflammatory colorectal carcinogenesis induced by treatment with azoxymethane and dextran sodium sulfate (AOM-DSS). The

Figure 1. IFNAR1 Levels and Signaling Are Reduced in Colorectal Adenocarcinomas

- (A) Heatmap and gene set enrichment analysis (GSEA) of IFN signaling pathway genes of the transcriptome profiles of human normal colon and matched CRC tissues (from Rohr et al., 2013). ES, enrichment score; NES, non-enrichment score; FDR, false discovery rate; FWER, family-wise error rate.
- (B) Representative immunofluorescent analysis of phospho-Tyr-STAT2 (red) and pan-cytokeratin (CK, green) in normal and malignant colon tissues counterstained with DAPI (blue). Boxplot showing nuclear pTyr-Stat2 levels in representative normal ($n = 8$) and cancer ($n = 11$) cases indicates median (dark line), 25%–75% range (box), minimum and maximum values (whiskers), and individual scatterplot values (circles) overlaying the boxplot.
- (C) Representative chromogen immunohistochemistry analysis of IFNAR1 in normal and malignant colon. Arrows point to IFNAR1-positive fibroblasts (black), epithelial cells (blue), and immune cells (red). Boxplots as in (B) show cytoplasmic IFNAR1 expression levels in the epithelial (left) or stromal (right) compartments of malignant colon and adjacent normal tissue.
- (D) Kaplan-Meier plot of cases of colorectal adenocarcinomas based on levels of cytoplasmic IFNAR1.
- (E) IFNAR1 (red)- and GLUT1 (green)-positive cells in normal and malignant human colon tissues. See also Figure S1.

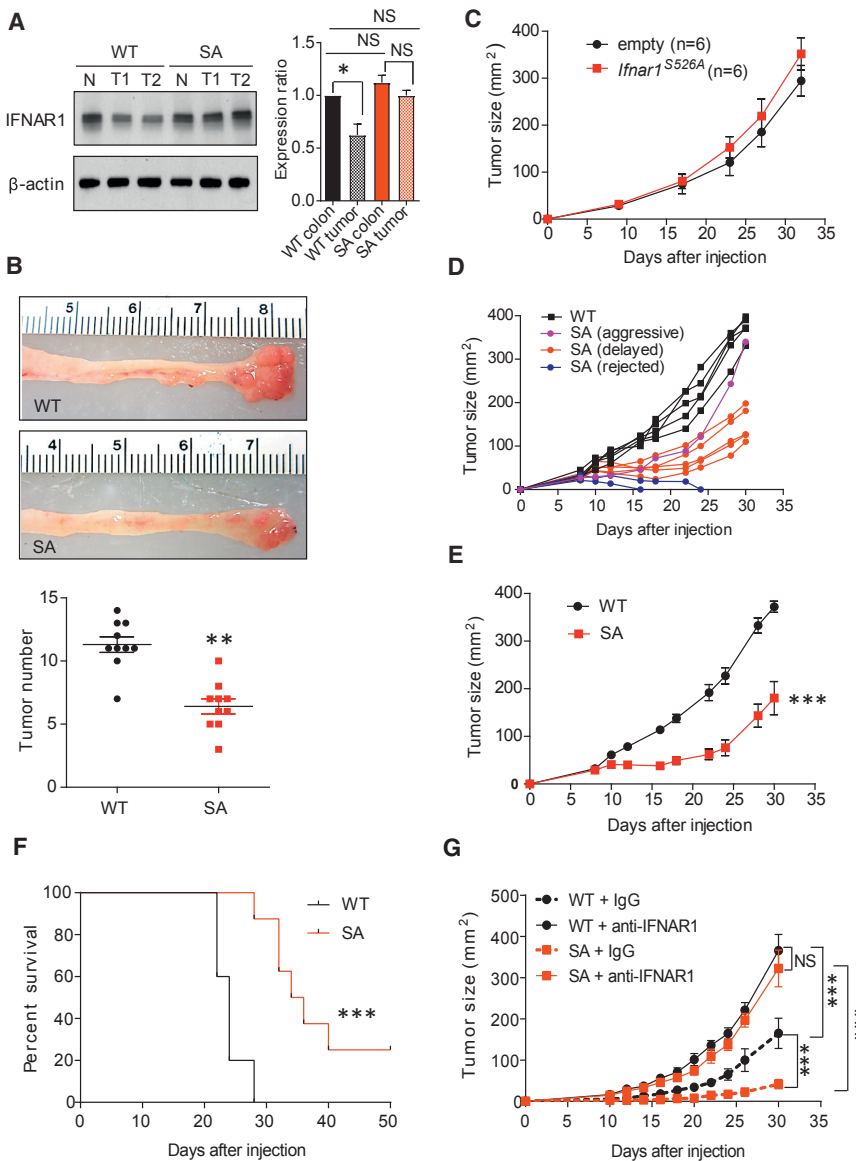


Figure 2. Downregulation of IFNAR1 in the Stromal Compartment Stimulates Colorectal Tumorigenesis

(A) Immunoblot analysis of IFNAR1 immunoprecipitated from the whole-tissue lysates prepared from normal colon or AOM-DSS-induced tumors from WT and SA mice. The IFNAR1/β-actin (loading control) signal relative ratios calculated from six mice for each group (WT colon taken as 1.0 and shown as mean ± SD) are depicted on the right. Henceforth asterisks: *p < 0.05; **p < 0.01; ***p < 0.001. NS, not significant.

(B) Representative images and quantification of colorectal tumors in mice of indicated genotypes at day 70 after treatment with AOM-DSS.

(C) Growth of MC38mRFP cells that received GFP or IFNAR1^{S526A}-GFP constructs after subcutaneous injection into WT mice (mean ± SEM, n = 6).

(D) Subcutaneous growth of individual MC38 tumors in WT and SA mice.

(E) A representative experiment demonstrating the average size of MC38 tumors growing in WT (n = 5) and SA (n = 8) mice (mean ± SEM).

(F) Kaplan-Meier analysis of the survival of MC38 tumor-bearing WT and SA mice from (E).

(G) Effect of anti-IFNAR1 neutralizing antibodies on MC38 tumor growth in WT and SA mice (mean ± SEM, n = 5–6 for each of two experiments).

See also Figure S2.

observed decrease in levels of IFNAR1 protein (Figures 2A and S2A) but not *Ifnar1* mRNA (Figure S2B) in AOM-DSS-induced colorectal tumors suggested an increased IFNAR1 degradation within tumors. Therefore, we next used *Ifnar1*^{S526A} mice (henceforth “SA”), previously shown to be deficient in IFNAR1 ubiquitination and degradation (Bhattacharya et al., 2014). SA mice treated with AOM-DSS sustained high levels of IFNAR1 protein (Figures 2A and S2A) and mRNA for IFN-stimulated and inflammatory genes (Figure S2C) relative to wild-type (WT) mice. Importantly, AOM-DSS treatment induced fewer tumors in SA mice (Figure 2B), indicating that downregulation of IFNAR1 contributes to efficient colorectal tumorigenesis.

In a transplantation model, tumors formed in WT mice by MC38 colon adenocarcinoma cells expressed lower levels of IFNAR1 compared with these cells cultured *in vitro* (Figure S2D), demonstrating that the MC38 tumor model re-capitulates the IFNAR1 loss observed in human CRC. To determine the im-

portance of IFNAR1 downregulation in the malignant cell compartment, we next aimed to restore IFNAR1 levels in MC38 cancer cells. Previous studies in fibrosarcomas and mammary adenocarcinomas demonstrated a tumor-suppressive effect of the IFN signaling in malignant cells (Bidwell et al., 2012; Sistigu et al., 2014). We also reported that expression of the *Ifnar1*^{S526A} allele in *Ifnar1*-null mouse melanoma cell line delays growth of these tumors (Katlinskaya et al., 2016). However, expression of the *Ifnar1*^{S526A} allele

in MC38mRFP cells did not affect their ability to form tumors in WT mice (Figures 2C, S2E, and S2F), indicating that the cell-autonomous anti-tumorigenic effects of IFNAR1 expression and IFN signaling might be cell or tumor type specific.

To determine the role of IFNAR1 downregulation in the stromal compartment, we inoculated WT or SA mice with MC38 cells (Figure S2G). While WT mice readily supported tumor growth, very few of MC38 tumors grew aggressively in SA mice (Figure 2D). Notably, most of these tumors were either rejected or exhibited a delayed growth (Figures 2D, 2E, and S2H) resulting in a prolonged survival (Figure 2F) in SA mice, suggesting an important role of downregulation of stromal IFNAR1 in tumorigenesis. Indeed, injection of IFNAR1-neutralizing antibodies further stimulated MC38 tumor growth in WT mice and dramatically rescued tumor growth in SA hosts (Figure 2G). These results indicate that efficient tumor growth requires downregulation of IFNAR1 levels primarily in the non-malignant cells.

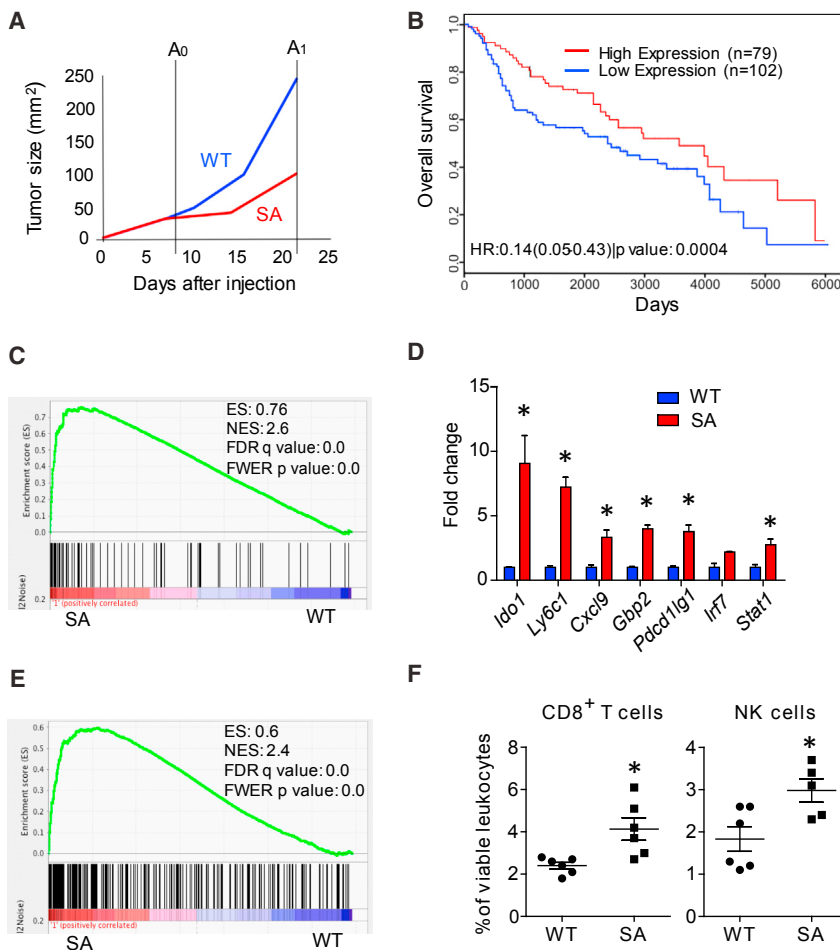


Figure 3. Alterations of Gene Expression Associated with IFNAR1 Downregulation Correlate with Local Immunosuppression and with a Poor Prognosis in CRC Patients

(A) Schematic representation of MC38 tumor growth in WT and SA mice. Time points of harvesting tumors of comparable (A0) and disparate (A1) size are indicated.

(B) Survival of adjusted for stage CRC patients (GEO: GSE41258) harboring the expression pattern of 30 selected genes similar to MC38 that grew either in WT (blue) or in SA (red) mice.

(C) GSEA results of the IFN- α/β signaling pathway in tumors harvested at day 9 (time point A0) and used for RNA isolation and microarray analysis.

(D) qPCR analysis of the indicated genes expressed in WT and SA tumors.

(E) GSEA results for the immune system process in tumors harvested at A0.

(F) Percent of NK and CD8 $^{+}$ T cells (relative to CD45 $^{+}$ cells) infiltrating MC38 tumors in WT and SA mice. Data are shown as mean \pm SEM from five to six tumors.

See also Figure S3 and Table S1.

Alterations of Gene Expression Associated with IFNAR1 Downregulation Correlate with Local Immunosuppression and Poor Prognosis in CRC Patients

We next profiled the gene expression associated with IFNAR1 downregulation (in tumors with WT stroma) or stabilized IFNAR1 (in tumors with SA stroma). Notably, at an early time point after MC38 transplantation (A0, Figure 3A), the stromal compartments from tumors of comparable size that arose in WT or SA mice already differed in their gene expression patterns (Table S1). While most of differentially expressed genes (e.g., *Ifit1*, *Ifit2*, *Mx2*, *Usp18*, etc.) are well known to be induced by IFN, others (*Clec7a*, *Sdc3*) have not been previously reported as bona fide IFN-regulated genes in global expression studies (Mostafavi et al., 2016; Rusinova et al., 2013), suggesting that downregulation of IFNAR1 in the context of a growing tumor may elicit a more complex response than merely an IFN-signaling suppression. Specifically, the status of a set of 30 genes whose expression was increased in the stroma of early mouse SA tumors compared with WT ones (Table S1) was associated with impaired tumor progression in SA mice (Figures 2D, 2E, and S2H).

More importantly, this gene expression profile was also predictive of a better prognosis in two separate stage-adjusted co-

horts of human CRC patients (Figures 3B and S3A). Furthermore, dramatic suppression of the IFN-induced genes (Figures 3C and 3D) correlated with subsequent aggressive tumor growth (Figure 2D) was seen in early WT (but not SA) tumors. These data suggest that IFNAR1 downregulation and the ensuing alterations in gene expression contribute to CRC progression and appear to be predictive of disease outcome in human CRC patients.

Additional comparison of WT and SA gene expression patterns revealed a suppressed immune pathway in early WT tumors (Figures 3D and 3E) pointing to the immune system as a putative target of IFNAR1 downregulation. At later time points, when tumors in WT mice became larger than tumors in SA mice (A1, Figure 3A), we noted a similar suppression of IFN signaling and in the signature of immune genes in WT tumors (Figures S3B and S3C). These results indicate that decreased IFNAR1 levels in the stromal compartment may determine both the immunosuppressive capacity and growth potential of the tumor.

Prompted by gene expression data we assessed the levels of immune cells in WT and SA mice burdened with MC38 tumors. Compared with SA mice, spleens from WT mice contained somewhat greater overall levels of CD11b $^{+}$ Ly6G $^{+}$ cells; however, we did not detect significant differences in the frequencies of splenic natural killer (NK) cells or T cells (Figure S3D) that would be characteristic of generalized immunosuppression in tumor-bearing WT animals. Conversely, analysis of tumor-infiltrating leukocyte subsets revealed significantly reduced frequencies of CD8 $^{+}$ T cells, NK cells, and Ly6C hi Ly6G $^{-}$ cells in tumors from WT animals compared with tumors from SA mice (Figures 3F and S3E). This result indicates that downregulation of IFNAR1 within WT tumors is associated with a localized intra-tumoral

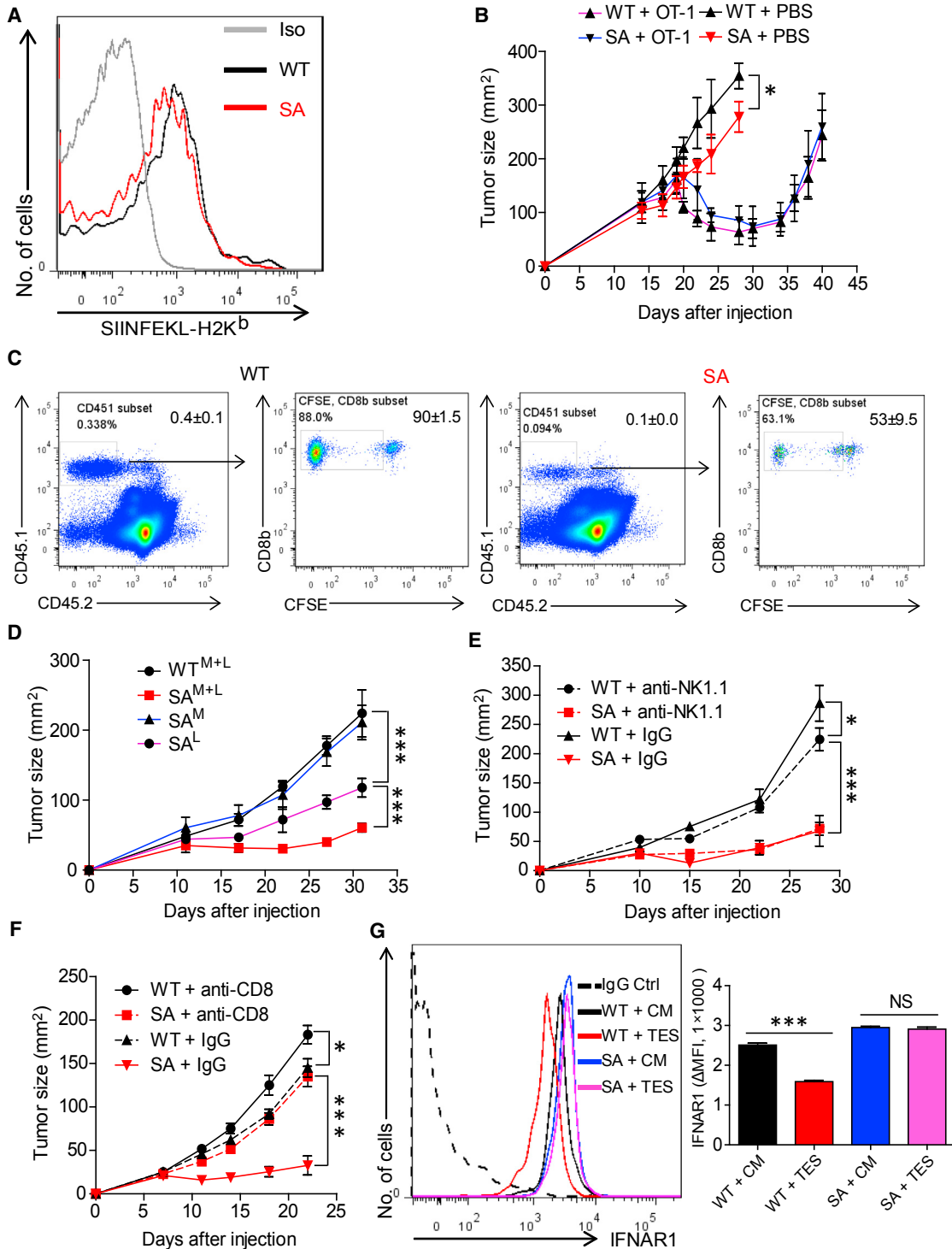


Figure 4. Downregulation of IFNAR1 on CTls Promotes Tumor Growth

(A) Representative fluorescence-activated cell sorting (FACS) analysis of levels of MHC-I-complexed OVA peptide on the surface of intra-tumoral CD45⁺MHC-II⁺CD103⁺CD11c⁺ DCs isolated from the MC38OVA tumors grown in *Rag1*^{-/-} mice harboring WT or SA IFNAR1.

(B) Growth of MC38-OVA tumors in *Rag1*^{-/-} mice harboring WT or SA IFNAR1 after adoptive transfer of WT OT-1 T cells injected on day 18 after tumor inoculation.

(C) Representative flow cytometry analysis of the percentage (left panels) and proliferation (right panels) of CD8⁺CD45.1⁺ at day 7 in the spleens from WT and SA mice after adoptive transfer of naive carboxyfluorescein succinimidyl ester (CFSE)-labeled OT-1 T cells at day 0 and subsequent challenge with MC38OVA cells at day 1.

(legend continued on next page)

immunosuppression, resulting in reduced CTL accumulation within the TME.

Downregulation of IFNAR1 in CTLs Contributes to Development of the Immunosuppressive TME in CRC

Previous studies of sarcomas and melanomas grown in WT or *Ifnar1* knockout mice suggested a critical role of IFN in the ability of specific CD8 α^+ lineage DCs to cross-present antigen to the CD8 $^+$ cytotoxic lymphocytes and highlighted the critical role of these DCs in anti-tumor immune protection (Diamond et al., 2011; Fuertes et al., 2011; Hildner et al., 2008). We did not observe changes in the overall frequency of intra-tumoral CD11b $^+$ CD11c $^+$ MHC-II $^+$ CD103 $^-$, CD11c $^+$ MHC-II $^+$ CD8 α^+ , or CD11c $^+$ MHC-II $^+$ CD103 $^+$ DCs between MC38 tumors that grew in WT and SA mice (Figure S3E). DCs isolated from WT or SA mice exhibited a similar efficacy in direct antigen presentation (Figure S4A) as well as in cross-presentation of tumor antigens (Figure S4B), indicating that reduced tumorigenesis in SA mice cannot be readily explained by an increased antigen presentation capacity.

We next transplanted MC38 tumor cells ectopically expressing ovalbumin (OVA) (MC38OVA) into immune-deficient *Rag1* $^{-/-}$ mice that harbored either WT or SA IFNAR1. Dendritic cells (CD45 $^+$ MHC-II $^+$ CD103 $^+$ CD11c $^+$) isolated from either WT or SA tumors presented comparable levels of MHC-I-complexed OVA peptide (Figure 4A). Consistent with these data, adoptive transfer of WT OVA-specific OT-1 CTLs into these *Rag1* $^{-/-}$ mice resulted in an initial decrease in tumor volume (followed by subsequent re-growth of tumors) regardless of IFNAR1 status (Figure 4B).

We next injected WT or SA mice with naive OT-1 T cells followed by challenge with MC38OVA and subsequent assessment of numbers and proliferation of splenic OT-1 CD8 $^+$ T cells 6 days later. Under these conditions, even less CTL proliferation was seen in the SA hosts compared with WT mice (Figure 4C), further indicating that the tumor growth defect observed in SA mice is unlikely to depend on increased antigen presentation by SA DCs.

We next generated mixed bone marrow chimeras in which myeloid and/or lymphoid cells from either WT or SA animals were used to reconstitute bone marrow in lethally irradiated WT mice (Diamond et al., 2011). These chimeric mice harbored comparable numbers of myeloid and lymphoid cells and the expected IFNAR1 levels on these cells in the spleen (Figure S4C). A dramatic suppression of MC38 tumor growth observed in chimeras that received both lymphoid and myeloid cells from SA donors ("SA $^{M+L}$," Figures 4D and S4D) was indicative of the critical importance of IFNAR1 downregulation in the bone marrow-derived cells. Relative to this group, only a slight acceleration of tumorigenesis was seen in mice that received WT myeloid cells and SA lymphocytes ("SA L "). This result indicates that, while

there is a role for IFNAR1 expressed on myeloid cells, maintaining the levels of IFNAR1 on lymphocytes appears to be critical for tumor growth suppression.

Indeed, while depletion of NK cells in SA mice did not alter growth of MC38 tumors (Figures 4E and S4E), depletion of CD8 $^+$ cells notably stimulated tumor growth in SA animals (Figures 4F and S4F). We next sought to determine whether IFNAR1 can be downregulated specifically on the intra-tumoral CD8 $^+$ T cells. Incubation of WT (but not SA) CD8 $^+$ T cells with the tumor explant supernatant (Figure 4G) or MC38 cell-conditioned medium (Figure S4G) robustly downregulated IFNAR1 cell surface levels. Together with notably lower levels of IFNAR1 on the surface of CD3 $^+$ CD8 $^+$ WT (but not SA) cells isolated from tumors compared with those isolated from spleens (Figure S4H), these data suggest that tumor conditions trigger downregulation of IFNAR1 on the surface of CTLs and that this downregulation contributes to aggressive tumorigenesis.

The majority of cells expressing high levels of IFNAR1 in normal human colon were CD3 $^+$ cells (Figure S5A). Importantly, in human CRC tissues, most IFNAR1-positive T lymphocytes were peripheral to the tumor and very few of them were found inside human tumors (Figures 5A and S5B). Whereas these low numbers of CTLs found in human CRC could be recapitulated in MC38 tumors grown in WT mice, a greater absolute and relative number of the CD3 $^+$ CD8 $^+$ CTLs was found within tumors developed in SA animals (Figures 3F and 5B). Consistent with this result, mouse SA tumors exhibited a prominent T cell gene expression signature (Figure 5C) and particularly high levels of mRNA of genes indicative of T cell effector function including *Ifng* and *Gzmb* (Figure S5C), as well as increased levels of IFN- γ and granzyme B proteins in MC38 tumor lysates (Figure S5D). Likewise, greater levels of *Ifng* mRNA expression were also observed in SA tumors induced by AOM-DSS treatment compared with WT tumors (Figure S2C). These results suggest that reduced accumulation of CTLs (indicative of immune-privileged niche) in CRC is associated with IFNAR1 downregulation.

Accordingly, studies involving adoptive transfer of CD8 $^+$ T cells into *Rag1* $^{-/-}$ mice burdened with MC38OVA tumors revealed a greater intra-tumoral accumulation of CTLs derived from SA OT-1 mice compared with CTLs from WT OT-1 animals (Figure 5D). These results suggest that the status of IFNAR1 on CTLs determines their ability to accumulate within tumors. These findings in human and mouse tumors collectively indicate that the IFNAR1 downregulation on CTLs that occurs within CRC tumors prevents CTL accumulation, thereby establishing a local immune-privileged TME.

Given that little, if any, difference was detected in proliferation of SA and WT CD8 $^+$ T lymphocytes activated in vitro (Figure S5E) or isolated from tumor-bearing mice (Figure S5F), we next focused on other mechanisms that could explain preferential

(D) Growth of MC38 tumors in *Rag1* $^{-/-}$ mice that received bone marrow containing WT or SA myeloid and lymphoid cells (WT $^{M+L}$ and SA $^{M+L}$), WT myeloid and SA lymphoid cells (SA L), or WT lymphoid and SA myeloid cells (SA M).

(E) MC38 tumor growth in WT or SA mice treated with anti-NK.1.1 or immunoglobulin G (IgG) control antibodies.

(F) MC38 tumor growth in WT or SA mice treated with anti-CD8 or IgG control antibodies.

(G) Representative FACS analysis and quantification ($n = 4$, each in triplicate) of IFNAR1 levels on the surface of CD3 $^+$ CD8 $^+$ cells isolated from WT or SA spleens and incubated in vitro with control medium (CM) or tumor explant supernatant (TES) for 2 hr. NS, not significant.

Data depicted as mean \pm SEM ($n = 4\text{--}6$); similar results were obtained in at least two independent experiments.

See also Figure S4.

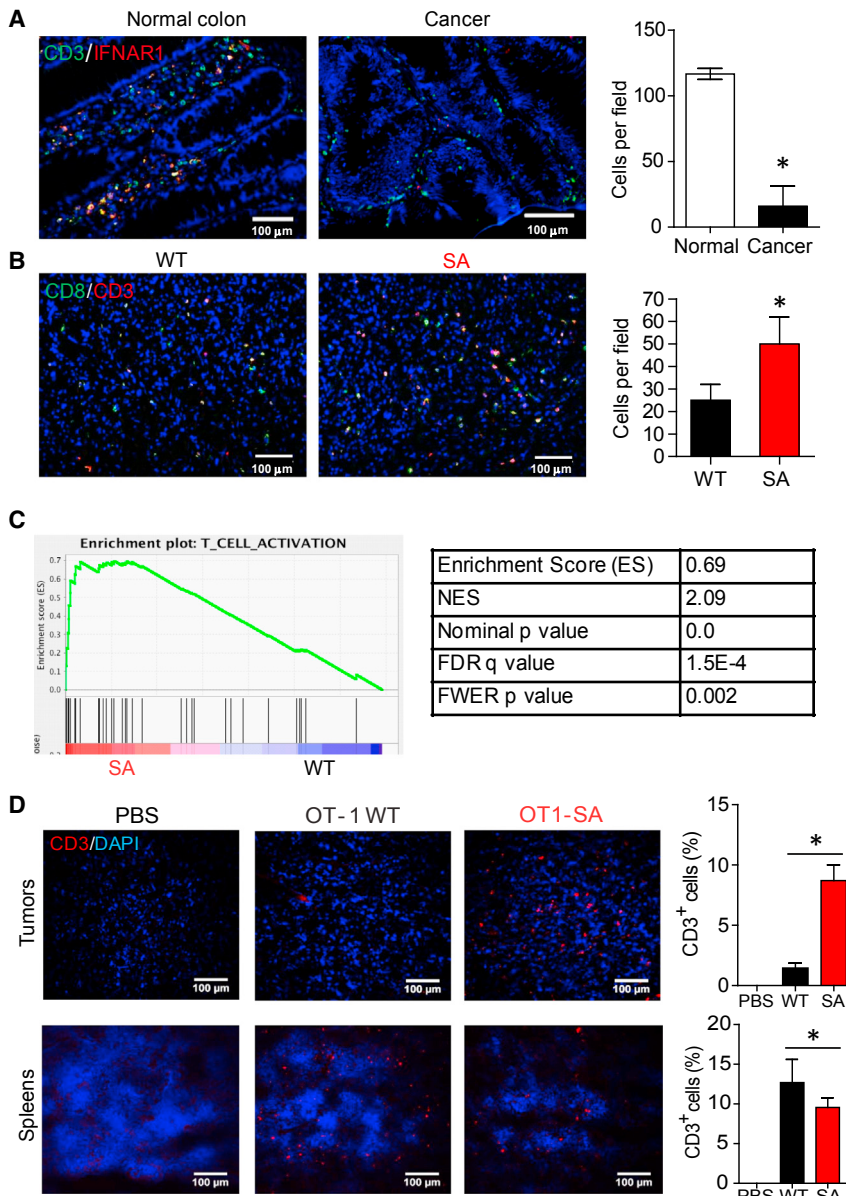


Figure 5. Downregulation of IFNAR1 in CTLs Contributes to Development of the Immunosuppressive Tumor Microenvironment in CRC

(A) Representative immunofluorescent analysis and quantification of IFNAR1^{hi}CD3⁺ T cell infiltration of human normal colon and CRC. Tissue sections were stained with antibodies against IFNAR1 (red) and CD3 (green) and contrasted with DAPI (blue). At least 20 randomly chosen fields from each of eight patient samples for each group were quantified.

(B) Representative immunofluorescent analysis and quantification of CD3⁺CD8⁺ T cell infiltration of MC38 tumors from WT and SA mice. Tumor sections were stained with anti-CD3 (red) and -CD8 (green) antibodies and contrasted with DAPI (blue). At least 20 randomly chosen fields from each of five tumor samples were quantified.

(C) GSEA results of the T cell activation gene signature in WT and SA tumors.

(D) Representative immunofluorescent analysis of T cells found in the spleens or MC38OVA tumors grown in *Rag1*^{-/-} mice after treating these mice with PBS or adoptive transfer of WT or SA OT-1 T cells (2×10^7 per mouse). Data are depicted as the percentage of CD3⁺ cells among all DAPI-stained cells and are representative of at least 20 random fields scored from tissues of four mice.

Data are shown as mean \pm SEM.

See also Figure S5.

CTL accumulation in tumors of SA mice. Cancer-associated fibroblasts positive for the fibroblast activation protein (FAP) produce CXCL12 chemokine that prevents intra-tumoral CTL buildup in a mouse pancreatic cancer model (Feig et al., 2013). Intriguingly, activated SA and WT CTLs exhibited a similar chemotaxis toward CXCL12 or CXCL9 (Figure S5G), suggesting that retaining IFN signaling may not necessarily increase the migratory abilities of CTLs.

Downregulation of IFNAR1 on CTLs Undermines Their Survival within the TME

IFN promotes survival of anti-viral CTLs by protecting them from killing by NK cells (Crouse et al., 2014; Xu et al., 2014). Depletion of NK cells in *Rag1*^{-/-} mice indeed increased the total number of transferred T cells but did not affect a greater viability of SA T cells compared with WT T cells (Figure S6). Given this result

and the observation that NK depletion did not alter tumorigenesis in either WT or SA mice (Figure 4E), we focused on other mechanisms by which downregulation of IFNAR1 may affect anti-tumor CTLs. Antigen-exposed SA CTLs cultured in vitro maintained greater levels of IFNAR1, the mRNA, and the protein levels for the anti-apoptotic regulator, B cell lymphoma-extra large (Bcl-XL), and lower levels of cleaved caspase-3 compared with WT CTLs (Figures 6A and S7A). Accordingly, a decrease in cell viability was more pronounced in WT cells than in SA cells under these conditions (Figure 6B). Importantly, while pre-treatment with interleukin-2 (IL-2) increased the viability of WT CTLs, neutralizing the IL-2 receptor using anti-CD25 antibody undermined the survival of SA CTLs (Figure 6B). We further found that SA CTLs produced notably more IL-2 (Figure S7B) and expressed greater levels of IL-2R α mRNA and protein compared with WT cells (Figures S7C and S7D). Thus, it is likely that downregulation of IFNAR1 promotes death of activated CTLs by attenuating the pro-survival effects of the IL-2 pathway.

Activated SA OT-1 CTLs exhibited greater viability than WT OT-1 CTLs when these cells were simultaneously injected in a 1:1 ratio intravenously or directly into the MC38OVA tumors grown in *Rag1*^{-/-} mice (Figures 6C and 6D). This result suggests that stabilization of IFNAR1 on antigen-specific CTLs improves their survival within the tumors. To further corroborate this possibility, we used the CAR-based approach that involved the

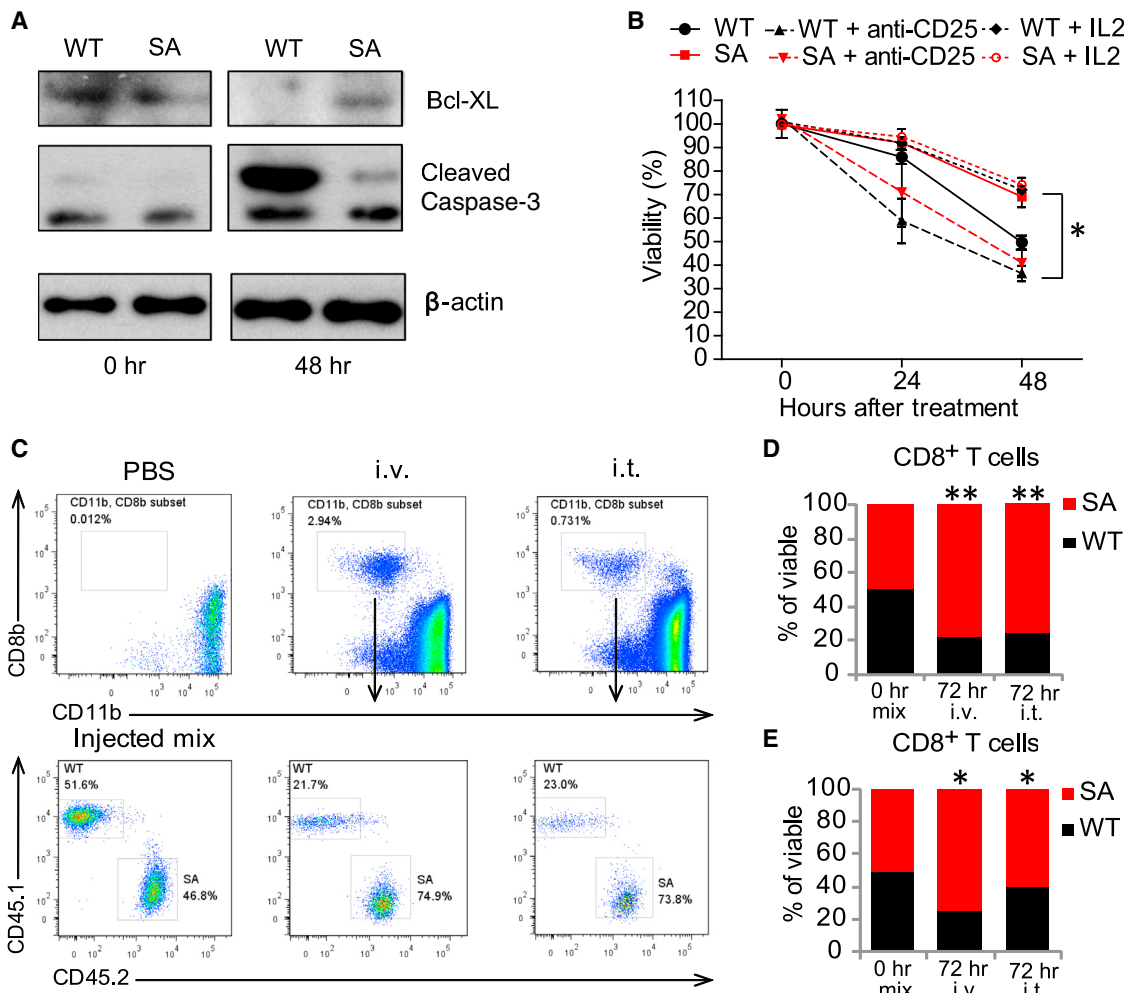


Figure 6. Downregulation of IFNAR1 on Cytotoxic T Lymphocytes Undermines their Survival within the TME

(A) Immunoblot analysis of Bcl-XL, cleaved caspase-3 levels, and β-actin (loading control) in splenocytes from WT and SA OT-1 mice activated with SIINFEKL peptide (0.5 µg/mL for 48 hr) and then cultured for indicated times.

(B) Viability of activated CD3⁺CD8⁺ cells in the presence of medium supplemented or not with either IL-2 (100 U/mL) or anti-CD25 antibody (100 µg/mL), as indicated, was determined by flow cytometry analysis after the indicated times. Mean ± SD (triplicates per mouse spleen, average from three mice) are shown. Asterisks denote statistical significance ($p < 0.05$) between WT and SA, between WT and WT treated with IL-2, and between SA and SA treated with anti-CD25 antibody.

(C) Flow cytometry analysis of the fraction of viable OT-1 WT (CD45.1) or SA (CD45.2) CTLs in the MC38OVA tumors 72 hr after intravenous (i.v.) injection (1:1 ratio) or directly into the tumors (i.t.) of *Rag1*^{-/-} mice bearing MC38OVA tumors.

(D) Quantitation of the experiments shown in (C) (mean percentage of viable cells from tumors from three to five mice). Similar results were obtained in at least two independent experiments.

(E) Quantitation of flow cytometry analysis of the fraction of viable FAP-CAR EGFP⁺ WT (CD45.1) or EGFP⁺ SA (CD45.2) CTLs in the MC38 tumors 72 hr after i.v. injection (1:1 ratio) or directly into the tumors (i.t.) of WT MC38 tumor-bearing mice. Data are shown as the mean percentage of viable cells ($n = 5$).

See also Figures S6 and S7.

introduction of the CAR against FAP (FAP-CAR [Wang et al., 2014]) into WT or SA CTLs. We generated FAP-CAR T cells separately from WT or SA lymphocytes, and then mixed these cells in equal parts prior to adoptive transfer (as a 1:1 mixture) into MC38 tumor-bearing WT mice (Figure S7E). Regardless of the route of administration (intra-tumoral or intravenous), a greater fraction of SA cells was found in the tumor 3 days later (Figures 6E and S7F). These results suggest that TME-induced downregulation of IFNAR1 on CTLs compromises the viability of these CTLs inside tumors.

Downregulation of IFNAR1 in CTLs Limits the Efficacy of Anti-cancer Therapies

We next examined the importance of IFNAR1 downregulation in modulating the efficacy of adoptive CTL transfer-based immunotherapy. Adoptive transfer of WT OT-1 lymphocytes into *Rag1*^{-/-} mice bearing MC38OVA tumors was much less efficient in sustained suppression of tumor growth and prolonging animal survival compared with SA OT-1 cells (Figures 7A and 7B). Furthermore, FAP-CAR CTLs prepared from SA cells exhibited a substantially greater therapeutic effect against MC38 tumors

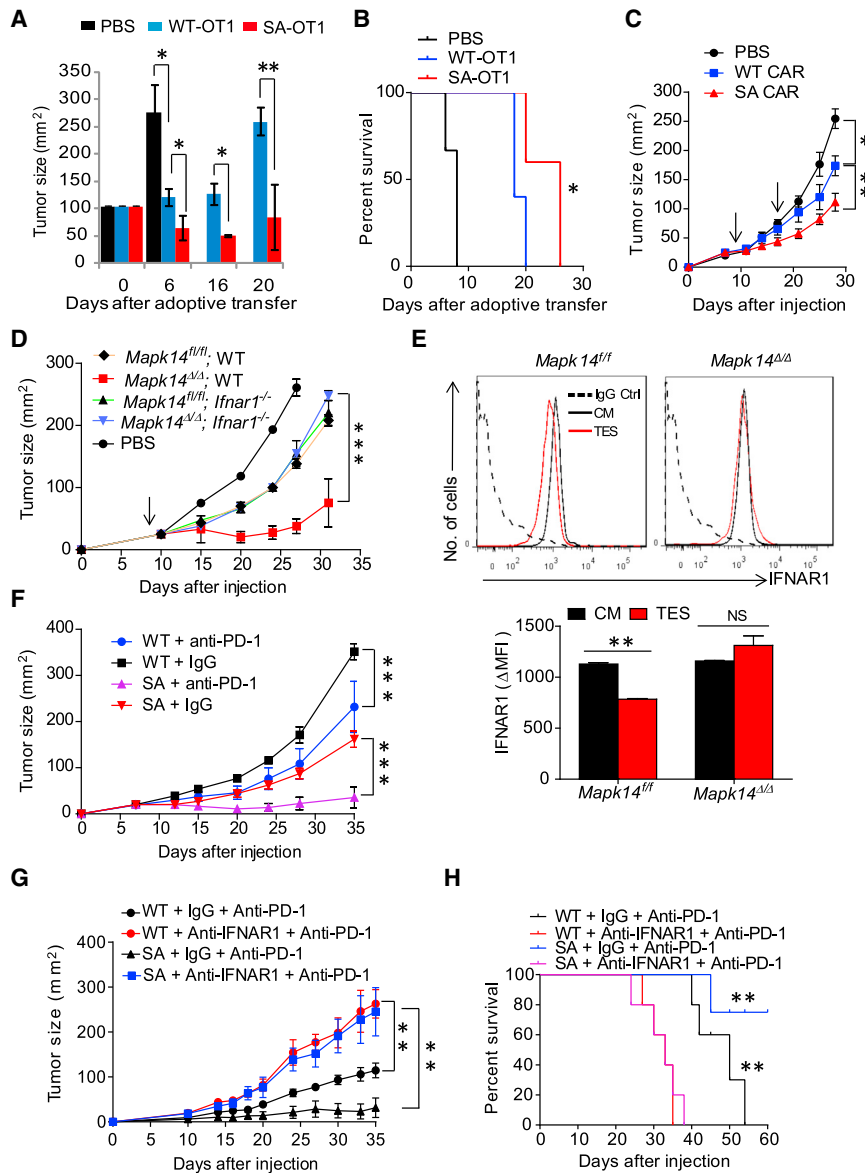


Figure 7. Downregulation of IFNAR1 in CTLs Limits the Efficacy of Immunotherapies

(A) Anti-tumor effects of adoptively transferred OT-1-SA and OT-1 WT T cells in MC38OVA tumor-bearing *Rag1*^{-/-} described in Figure 5D.

(B) Kaplan-Meier analysis of survival of MC38 tumor-bearing mice from (A)

(C) Anti-tumor effects of IFNAR1 WT and IFNAR1 SA FAP-CAR T cells (time of administration indicated by arrow) in MC38 tumor-bearing mice.

(D) Growth of MC38 tumors in WT mice that received PBS or FAP-CAR T cells harboring indicated status of *Mapk14* and *Ifnar1* shown.

(E) Cell surface IFNAR1 levels on CD3⁺CD8⁺ splenocytes of the indicated genotype treated with TES or CM for 2 hr. Representative FACS and quantitation (below) are shown.

(F) Anti-tumor effect of anti-PD-1 antibody administration in WT mice and SA mice bearing MC38.

(G) Effect of IFNAR1 neutralization on the efficacy of anti-PD-1 treatment of WT or SA mice bearing MC38 tumors.

(H) Kaplan-Meier analysis of survival of MC38 tumor-bearing mice from (G).

Data shown as mean ± SEM ($n = 3–5$) from each of at least two to three independent experiments.

ablation of *Ifnar1*, suggesting that most (if not all) effects of p38 α deletion depend on sustained IFNAR1 signaling within CTLs (Figure 7D). Together with the inability of CTLs lacking p38 α to downregulate IFNAR1 in response to an in vitro treatment with the tumor explant supernatant (Figure 7E), these data provide genetic evidence suggesting that tumor-derived factors-induced p38 α -dependent downregulation of IFNAR1 on the surface of CTLs limits the efficacy of CAR-based therapeutics in solid tumors.

Intriguingly, a fraction of MC38 tumors that did not get rejected in SA mice even-

ually reached a larger size (A1, Figure 3A). Whereas SA tissues retained a greater immune response and robust IFN signatures, there was also a notable increase in expression of the PD-L1/CD274 checkpoint molecule (Figure S3C). Accordingly, treatment with the anti-PD-1 antibody at a dose that only slightly delayed MC38 tumor growth in WT mice caused a robust therapeutic effect leading to a stable disease in SA mice (Figure 7F). Importantly, anti-PD-1 therapy was notably less efficient in suppressing tumor growth (Figure 7G) and improving animal survival (Figure 7H) in SA mice that also received anti-IFNAR1 neutralizing antibody. These data collectively suggest that downregulation of IFNAR1 undermines the efficacy of checkpoint-targeted immunotherapeutics against solid tumors.

We noted a greater phosphorylation of p38 α in lysates from MC38 tumors relative to cultured MC38 cells (Figure 8A), consistent with activation of p38 α by TME stress. Accordingly, we next examined whether downregulation of IFNAR1 can be reversed

relative to FAP-CAR WT CTLs (Figure 7C). The magnitude of these effects is probably underappreciated because the SA allele may inhibit proliferation of CAR CTLs (data not shown), and FAP-CAR SA cells used in these experiments were likely to partially suppress IFN signaling downstream of the receptor.

To overcome this problem we sought to acutely stabilize IFNAR1 via inducible ablation of p38 α , a kinase potentially involved in the ligand-independent downregulation of IFNAR1 (Bhattacharya et al., 2011). We prepared FAP-CAR T cells from the splenocytes of mice harboring floxed *Mapk14* (a gene that encodes p38 α), either *Ifnar1*^{+/+} (WT) or *Ifnar1*^{-/-} alleles, and either no Cre or inducible *Ubc9-Cre*^{ERT2}. These FAP-CAR T cells were treated with 4-hydroxytamoxifen and then injected into WT mice burdened with MC38 tumors. As seen from Figure 7D, inactivation of p38 α in IFNAR1-expressing FAP-CAR CTLs (*Mapk14*^{Δ/Δ} WT) dramatically increased the anti-tumor efficacy of these cells. Importantly, this increased effect could be negated by concurrent

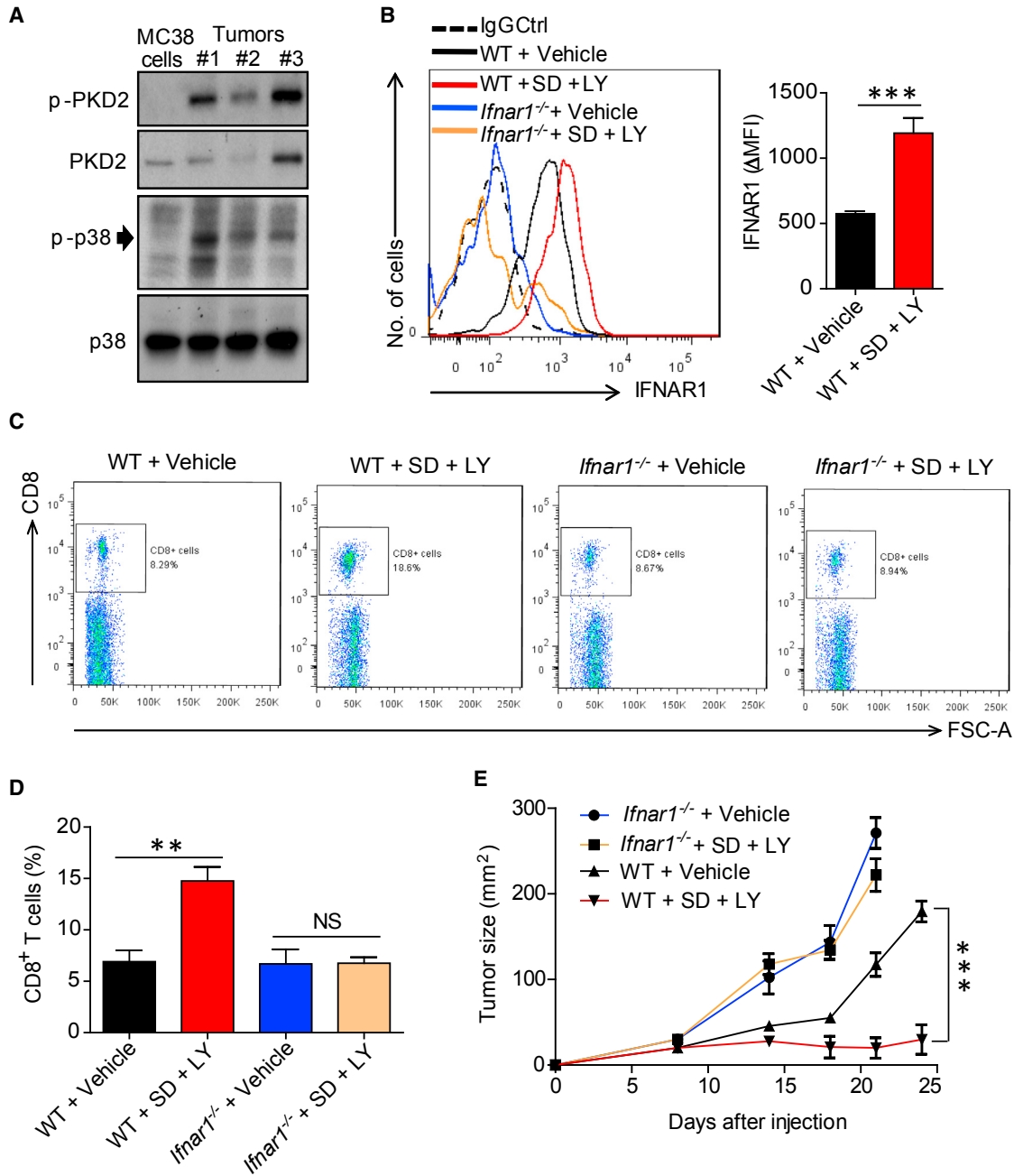


Figure 8. Pharmacologic Stabilization of IFNAR1 Disrupts Immune-Privileged Niche and Elicits a Therapeutic Effect against Tumors

(A) Immunoblot analysis of phosphorylation and levels of p38 α and PKD2 kinases in cultured MC38 cells and MC38 tumors.

(B) Levels of cell surface IFNAR1 on tumor-infiltrating CD3 $^{+}$ CD8 $^{+}$ cells isolated from MC38 tumors grown in WT or Ifnar1-null mice treated with kinase inhibitors as indicated. Representative FACS and quantification are shown.

(C) Frequency of CD8 $^{+}$ T cells (% of CD45 $^{+}$ cells) isolated from MC38 tumors grown in WT or Ifnar1-null mice treated with kinase inhibitors as indicated.

(D) Quantification of results shown in (C).

(E) Anti-tumor effect of SD-208 and LY2228820 administered to Ifnar1^{-/-} and WT mice bearing MC38 tumors as described in the [Experimental Procedures](#).

Data are shown as mean \pm SEM (n = 5 from each of three independent experiments).

See also [Figure S8](#).

by pharmacologic means. To this end, we attempted to stabilize IFNAR1 using the p38 inhibitor LY2228820 (LY). Given that some TME factors such as vascular endothelial growth factor can also downregulate IFNAR1 via activating protein kinase-2

(PKD2) (Zheng et al., 2011), and that PKD2 activity was indeed increased in MC38 tumors compared with cultured MC38 cells (Figure 8A), we combined the p38 inhibitor with SD-208 (SD), a PKD inhibitor.

The combination of these small molecules (LY + SD) prevented tumor explant supernatant-induced downregulation of IFNAR1 on CTLs *in vitro* (Figure S8A). Furthermore, *in vivo* treatment with this combination (which was well tolerated by tumor-bearing mice, Figure S8B), led to a notable increase in the overall levels of IFNAR1 within tumors (Figure S8C) and specifically of cell surface IFNAR1 levels on intra-tumoral CD3⁺CD8⁺ cells (Figure 8B). Remarkably, administration of LY + SD robustly increased numbers of CTLs found inside MC38 tumors that grew in WT but not in *Ifnar1*^{-/-} mice (Figures 8C, 8D, S8D, and S8E), suggesting that inhibition of p38 and PKD disrupts the immune-privileged niche within the TME in an IFNAR1-dependent manner.

Consistent with an important role of IFNAR1 downregulation in the stimulation of tumorigenesis, treatment with these kinase inhibitors dramatically suppressed growth of MC38 tumors in WT mice, but not in mice lacking *Ifnar1* (Figure 8E), indicating that stimulation of IFNAR1 signaling is a major mechanism underlying the immune-reactivating and anti-tumorigenic effects of these agents. In all, these results provide a proof of principle for pharmacologic stabilization of IFNAR1 as the means to attenuate local immunosuppression within tumors and to suppress tumor growth.

DISCUSSION

Delineating the mechanisms that impose localized immune suppression within the TME is essential for improving the efficacy of immunotherapeutics in solid tumors. Here we present evidence that links the TME stress-driven downregulation of IFNAR1 to the reduced viability of intra-tumoral CTLs and the ensuing establishment of an immune-privileged niche in CRC tumors. A decrease in IFNAR1 levels and expression of IFN-inducible genes found in human CRC tumors and recapitulated in mouse tumors is associated with the establishment of a localized niche virtually void of CTLs, as well as with robust tumor growth and poor prognosis. Downregulation of IFNAR1 specifically in CTLs induced by tumor-associated factors inhibits CTL viability and undermines the efficacy of immune therapies. Conversely, genetic or pharmacologic stabilization of IFNAR1 disrupts the immune-privileged niche, suppresses tumor growth, and increases the efficacy of CAR T cell therapy and immune checkpoint inhibitors.

These findings suggest that IFNAR1 downregulation contributes to the development and progression of CRC. While not arguing against additional role of IFNAR1 in IFN-modulated regulation of antigen presentation and activation of DCs (Diamond et al., 2011; Fuertes et al., 2011; Hildner et al., 2008), stromal resistance to tumor-induced angiogenesis (Zheng et al., 2011) and other processes, our current results strongly indicate that IFNAR1 downregulation on intra-tumoral CTLs contributes to the establishment of immune-privileged TME by undermining CTL survival. These results are consistent with an important role of IFN as an activation signal for T cells (Curtsinger et al., 2005) and the observation that insufficient “third signal” contributes to the inhibition of CTLs in solid tumors (Curtsinger et al., 2007). It appears that downregulation of IFNAR1 on CTL negatively affects responses of these CTLs to IL-2 pro-survival signals and, accordingly, stimulates pro-apoptotic pathways, although other mechanisms cannot be ruled out. Regardless of the exact

mechanisms, the data presented here argue for the development of therapeutic strategies aimed to stabilize IFNAR1 and improve CTL viability within solid tumors.

Our results specifically emphasize the importance of IFNAR1 downregulation on CTLs. Given the importance of these cells in anti-tumor immunity against diverse malignant lesions, it is likely that downregulation of IFNAR1 in the stromal compartment may stimulate growth and progression of other cancer types. Indeed, we have recently demonstrated that loss of IFNAR1 stimulates growth of transplanted melanomas (Katlinskaya et al., 2016). Overall, our data are consistent with intra-tumoral IFN production being linked with CTL generation and viability (Hiroishi et al., 2000), observations that IFN may act to improve the effect of adoptive transfer of CTLs (Hervas-Stubbs et al., 2012), and with recent finding that a specific CAR design, which serendipitously increased IFN signaling in CTLs, evoked an augmented therapeutic effect (Zhao et al., 2015). Nevertheless, our results do not rule out additional putative cellular targets (e.g., interleukin-10-expressing Treg cells; Stewart et al., 2013) and additional mechanisms by which elimination of IFNAR1 and suppression of IFN signaling can further contribute to localized immunosuppression and stimulation of solid tumors growth.

Previous studies utilizing chemically induced and transplantable sarcomas and melanomas in IFNAR1 knockouts have identified specific CD8⁺ DCs as targets of protective role of IFN against tumors (Diamond et al., 2011; Fuertes et al., 2011; Hildner et al., 2008). Functional defects of *Ifnar1*-null DCs reported in these studies are consistent with an important role of IFNAR1 in the maturation of DCs (Le Bon and Tough, 2002; Santini et al., 2009). We did not observe an increase in antigen presentation in SA mice. Furthermore, SA DCs might have a survival disadvantage given that elimination of IFNAR1 plays an important role in preserving the viability of IFN-expressing DCs exposed to inducers of pathogen recognition receptor signaling (Qian et al., 2011). Future use of SA animals in sarcoma and melanoma models is likely to reveal additional information on the relative contribution of IFNAR1 status in DCs and other leukocytes to anti-tumor immunity.

Genetic and pharmacologic studies described here provide a proof of principle for a focus on stabilization of IFNAR1 to increase the efficacy of immunotherapies against CRC and possibly other solid tumors. Whereas the mechanisms underlying the therapeutic effect of p38/PKD inhibitors are likely to be mediated by many cell types (in addition to CTLs), it is noteworthy that these inhibitors still act in an IFNAR1-dependent manner. In addition to targeting p38 and PKD kinases responsible for phosphorylation of IFNAR1 leading to recruitment of the SCF-βTrcp E3 ligase, it might be possible to inhibit this class of ligases. Cullin-dependent ligases (including SCF-βTrcp) can be targeted by inhibiting the NEDD9-activating enzyme; its selective inhibitor, MLN4924, is currently under clinical trials in solid tumors (Sarantopoulos et al., 2015). Additional studies on combining IFNAR1-stabilizing regimens with diverse immunotherapeutic approaches are currently in progress.

EXPERIMENTAL PROCEDURES

A detailed description of the procedures utilized in this work can be found in the [Supplemental Experimental Procedures](#). Use of pre-existing human

archival de-coded and de-identified CRC tissue arrays, previously collected under informed consent, and samples that could not be directly or indirectly linked to individual human subjects was exempt from institutional review. All animal experiments were approved by the Institutional Animal Care and Use Committee (IACUC) of the University of Pennsylvania and were carried out in accordance with the IACUC guidelines. All mice were on the C57BL/6 background and had water ad libitum and were fed regular chow. Mice were maintained in a specific pathogen-free facility in accordance with American Association for Laboratory Animal Science guidelines. Littermate animals from different cages were randomly assigned into the experimental groups. These randomized experimental cohorts were either co-housed or systematically exposed to the bedding of other groups to ensure equal exposure to the microbiota of all groups. Statistical analysis was performed using Microsoft or GraphPad Prism 7 software. Unpaired Student's t test was used for the comparison between two groups. One-way ANOVA or two-way ANOVA analysis followed by the Bonferroni post hoc test were used for the multiple comparisons. Repeated-measure two-way ANOVA (mixed-model) followed by the Bonferroni post hoc test was used for the analysis of tumor growth curve. A value of $p < 0.05$ was considered significant.

Data from the global expression profiling studies were collected with Illumina BeadStudio 3.1.1.0 software, and statistical analyses were conducted on the IlluminaGUI R-package. Gene sets from microarray data were analyzed for overlap with curated datasets (C5, H) in the MSigDB using the web interface available at <http://www.broadinstitute.org/gsea/msigdb/index.jsp>. The raw data have been deposited at NCBI (GEO: GSE76889).

For AOM-DSS colorectal carcinogenesis, co-housed experimental mice were intraperitoneally injected with 10 mg/kg azoxymethane (Sigma). A week later, they were supplied with tap water containing 2.5% dextran sodium sulfate (TdB Consultancy) for 7 days followed by 14 days of regular water. This cycle was repeated three times and mice were killed 2 weeks after the end of the last DSS cycle or at the end of 10 weeks. Colons were harvested, washed of feces with Dulbecco'sPBS, and slit open longitudinally to count tumors. Tumors were flash frozen in liquid nitrogen or embedded into optimal cutting temperature medium for subsequent analysis.

SUPPLEMENTAL INFORMATION

Supplemental Information includes Supplemental Experimental Procedures, eight figures, and one table and can be found with this article online at <http://dx.doi.org/10.1016/j.ccr.2017.01.004>.

AUTHOR CONTRIBUTIONS

S.Y.F., K.V.K., J.G., E.P., H.R., C.K., and J.A.D. designed the research; K.V.K., J.G., A.O., Y.V.K., R.C., C.J.C., S.B., D.P.B., M.G., A.R.P., P.C., and A.K.R. performed the experiments and interpreted the data; S.Y.F., K.V.K., J.G., E.P., H.R., C.K., and J.A.D. wrote the manuscript with the help of all authors.

ACKNOWLEDGMENTS

This work was supported by the NIH/NCI PO1 CA165997 grant (to J.A.D., C.K., and S.Y.F.), and RO1 CA092900 (to S.Y.F. and H.R.). Additional support from NIH/NCI T32 CA009140 (to K.V.K.) is also appreciated. We thank Ze'ev Ronai, Mark J. Smyth, Melissa Wong, Yibin Wang, Susan Weiss, and Susan Ostrand-Rosenberg for reagents, Sandra Pellegrini, Mathias Müller, Birgit Strobl, and the members of Gabrilovich, Fuchs, Diehl, Koumenis, Pear, and Minn labs for critical suggestions.

Received: May 23, 2016

Revised: September 15, 2016

Accepted: January 9, 2017

Published: February 13, 2017

REFERENCES

- Aichele, P., Unsöld, H., Koschella, M., Schweier, O., Kalinke, U., and Vucikuja, S. (2006). CD8 T cells specific for lymphocytic choriomeningitis virus require type I IFN receptor for clonal expansion. *J. Immunol.* **176**, 4525–4529.
- Bhattacharya, S., Qian, J., Tzimas, C., Baker, D.P., Koumenis, C., Diehl, J.A., and Fuchs, S.Y. (2011). Role of p38 protein kinase in the ligand-independent ubiquitination and down-regulation of the IFNAR1 chain of type I interferon receptor. *J. Biol. Chem.* **286**, 22069–22076.
- Bhattacharya, S., HuangFu, W.C., Dong, G., Qian, J., Baker, D.P., Karar, J., Koumenis, C., Diehl, J.A., and Fuchs, S.Y. (2013). Anti-tumorigenic effects of type I interferon are subdued by integrated stress responses. *Oncogene* **32**, 4214–4221.
- Bhattacharya, S., Katlinski, K.V., Reichert, M., Takano, S., Brice, A., Zhao, B., Yu, Q., Zheng, H., Carbone, C.J., Katlinskaya, Y.V., et al. (2014). Triggering ubiquitination of IFNAR1 protects tissues from inflammatory injury. *EMBO Mol. Med.* **6**, 384–397.
- Bidwell, B.N., Slaney, C.Y., Withana, N.P., Forster, S., Cao, Y., Loi, S., Andrews, D., Mikeska, T., Mangan, N.E., Samarajiva, S.A., et al. (2012). Silencing of Ifr7 pathways in breast cancer cells promotes bone metastasis through immune escape. *Nat. Med.* **18**, 1224–1231.
- Brahmer, J.R., Tykodi, S.S., Chow, L.Q., Hwu, W.J., Topalian, S.L., Hwu, P., Drake, C.G., Camacho, L.H., Kauh, J., Odunsi, K., et al. (2012). Safety and activity of anti-PD-L1 antibody in patients with advanced cancer. *N. Engl. J. Med.* **366**, 2455–2465.
- Chiba, T., Ohtani, H., Mizoi, T., Naito, Y., Sato, E., Nagura, H., Ohuchi, A., Ohuchi, K., Shiiba, K., Kurokawa, Y., and Satomi, S. (2004). Intraepithelial CD8+ T-cell-count becomes a prognostic factor after a longer follow-up period in human colorectal carcinoma: possible association with suppression of micrometastasis. *Br. J. Cancer* **91**, 1711–1717.
- Crouse, J., Bedenikovic, G., Wiesel, M., Ibberson, M., Xenarios, I., Von Laer, D., Kalinke, U., Vivier, E., Jonjic, S., and Oxenius, A. (2014). Type I interferons protect T cells against NK cell attack mediated by the activating receptor NCR1. *Immunity* **40**, 961–973.
- Curtsinger, J.M., Valenzuela, J.O., Agarwal, P., Lins, D., and Mescher, M.F. (2005). Type I IFNs provide a third signal to CD8 T cells to stimulate clonal expansion and differentiation. *J. Immunol.* **174**, 4465–4469.
- Curtsinger, J.M., Gerner, M.Y., Lins, D.C., and Mescher, M.F. (2007). Signal 3 availability limits the CD8 T cell response to a solid tumor. *J. Immunol.* **178**, 6752–6760.
- Diamond, M.S., Kinder, M., Matsushita, H., Mashayekhi, M., Dunn, G.P., Archambault, J.M., Lee, H., Arthur, C.D., White, J.M., Kalinke, U., et al. (2011). Type I interferon is selectively required by dendritic cells for immune rejection of tumors. *J. Exp. Med.* **208**, 1989–2003.
- Fearon, D.T. (2014). The carcinoma-associated fibroblast expressing fibroblast activation protein and escape from immune surveillance. *Cancer Immunol. Res.* **2**, 187–193.
- Feig, C., Jones, J.O., Kraman, M., Wells, R.J., Deonarine, A., Chan, D.S., Connell, C.M., Roberts, E.W., Zhao, Q., Caballero, O.L., et al. (2013). Targeting CXCL12 from FAP-expressing carcinoma-associated fibroblasts synergizes with anti-PD-L1 immunotherapy in pancreatic cancer. *Proc. Natl. Acad. Sci. USA* **110**, 20212–20217.
- Fuchs, S.Y. (2013). Hope and fear for interferon: the receptor-centric outlook on the future of interferon therapy. *J. Interferon Cytokine Res.* **33**, 211–225.
- Fuertes, M.B., Kacha, A.K., Kline, J., Woo, S.R., Kranz, D.M., Murphy, K.M., and Gajewski, T.F. (2011). Host type I IFN signals are required for antitumor CD8+ T cell responses through CD8 α + dendritic cells. *J. Exp. Med.* **208**, 2005–2016.
- Galon, J., Costes, A., Sanchez-Cabo, F., Kirilovsky, A., Mlecnik, B., Lagorce-Pages, C., Tosolini, M., Camus, M., Berger, A., Wind, P., et al. (2006). Type, density, and location of immune cells within human colorectal tumors predict clinical outcome. *Science* **313**, 1960–1964.
- Gilham, D.E., Debets, R., Pule, M., Hawkins, R.E., and Abken, H. (2012). CAR-T cells and solid tumors: tuning T cells to challenge an inveterate foe. *Trends Mol. Med.* **18**, 377–384.
- Hellström, I., Hellström, K.E., Pierce, G.E., and Yang, J.P. (1968). Cellular and humoral immunity to different types of human neoplasms. *Nature* **220**, 1352–1354.

- Hervas-Stubbs, S., Riezu-Boj, J.I., Gonzalez, I., Mancheno, U., Dubrot, J., Azpilicueta, A., Gabari, I., Palazon, A., Aranguren, A., Ruiz, J., et al. (2010). Effects of IFN- α as a signal-3 cytokine on human naïve and antigen-experienced CD8(+) T cells. *Eur. J. Immunol.* 40, 3389–3402.
- Hervas-Stubbs, S., Mancheno, U., Riezu-Boj, J.I., Larraga, A., Ochoa, M.C., Alignani, D., Alfaro, C., Morales-Kastresana, A., Gonzalez, I., Larrea, E., et al. (2012). CD8 T cell priming in the presence of IFN- α renders CTLs with improved responsiveness to homeostatic cytokines and recall antigens: important traits for adoptive T cell therapy. *J. Immunol.* 189, 3299–3310.
- Hildner, K., Edelson, B.T., Purtha, W.E., Diamond, M., Matsushita, H., Kohyama, M., Calderon, B., Schraml, B.U., Unanue, E.R., Diamond, M.S., et al. (2008). Batf3 deficiency reveals a critical role for CD8alpha+ dendritic cells in cytotoxic T cell immunity. *Science* 322, 1097–1100.
- Hiroishi, K., Tuting, T., and Lotze, M.T. (2000). IFN-alpha-expressing tumor cells enhance generation and promote survival of tumor-specific CTLs. *J. Immunol.* 164, 567–572.
- Huangfu, W.C., Qian, J., Liu, C., Liu, J., Lokshin, A.E., Baker, D.P., Rui, H., and Fuchs, S.Y. (2012). Inflammatory signaling compromises cell responses to interferon alpha. *Oncogene* 31, 161–172.
- Joyce, J.A., and Fearon, D.T. (2015). T cell exclusion, immune privilege, and the tumor microenvironment. *Science* 348, 74–80.
- Katilinskaya, Y.V., Katilinski, K.V., Yu, Q., Ortiz, A., Beiting, D.P., Brice, A., Davar, D., Sanders, C., Kirkwood, J.M., Rui, H., et al. (2016). Suppression of type I interferon signaling overcomes oncogene-induced senescence and mediates melanoma development and progression. *Cell Rep* 15, 171–180.
- Klemm, F., and Joyce, J.A. (2015). Microenvironmental regulation of therapeutic response in cancer. *Trends Cell Biol.* 25, 198–213.
- Kolumam, G.A., Thomas, S., Thompson, L.J., Sprent, J., and Murali-Krishna, K. (2005). Type I interferons act directly on CD8 T cells to allow clonal expansion and memory formation in response to viral infection. *J. Exp. Med.* 202, 637–650.
- Kumar, K.G., Tang, W., Ravindranath, A.K., Clark, W.A., Croze, E., and Fuchs, S.Y. (2003). SCF(HOS) ubiquitin ligase mediates the ligand-induced down-regulation of the interferon-alpha receptor. *EMBO J.* 22, 5480–5490.
- Le Bon, A., and Tough, D.F. (2002). Links between innate and adaptive immunity via type I interferon. *Curr. Opin. Immunol.* 14, 432–436.
- Liu, J., HuangFu, W.C., Kumar, K.G., Qian, J., Casey, J.P., Hamanaka, R.B., Grigoriadou, C., Aldabe, R., Diehl, J.A., and Fuchs, S.Y. (2009). Virus-induced unfolded protein response attenuates antiviral defenses via phosphorylation-dependent degradation of the type I interferon receptor. *Cell Host Microbe* 5, 72–83.
- Marotta, D., Karar, J., Jenkins, W.T., Kumanova, M., Jenkins, K.W., Tobias, J.W., Baldwin, D., Hatzigeorgiou, A., Alexiou, P., Evans, S.M., et al. (2011). In vivo profiling of hypoxic gene expression in gliomas using the hypoxia marker EF5 and laser-capture microdissection. *Cancer Res.* 71, 779–789.
- Mostafavi, S., Yoshida, H., Moodley, D., LeBoite, H., Rothamel, K., Raj, T., Ye, C.J., Chevrier, N., Zhang, S.Y., Feng, T., et al. (2016). Parsing the interferon transcriptional network and its disease associations. *Cell* 164, 564–578.
- Naito, Y., Saito, K., Shiiba, K., Ohuchi, A., Saigenji, K., Nagura, H., and Ohtani, H. (1998). CD8+ T cells infiltrated within cancer cell nests as a prognostic factor in human colorectal cancer. *Cancer Res.* 58, 3491–3494.
- Platanias, L.C. (2005). Mechanisms of type-I- and type-II-interferon-mediated signalling. *Nat. Rev. Immunol.* 5, 375–386.
- Qian, J., Zheng, H., Huangfu, W.C., Liu, J., Carbone, C.J., Leu, N.A., Baker, D.P., and Fuchs, S.Y. (2011). Pathogen recognition receptor signaling accelerates phosphorylation-dependent degradation of IFNAR1. *PLoS Pathog.* 7, e1002065.
- Quail, D.F., and Joyce, J.A. (2013). Microenvironmental regulation of tumor progression and metastasis. *Nat. Med.* 19, 1423–1437.
- Rohr, C., Kerick, M., Fischer, A., Kuhn, A., Kashofer, K., Timmermann, B., Daskalaki, A., Meinel, T., Drichel, D., Borno, S.T., et al. (2013). High-throughput miRNA and mRNA sequencing of paired colorectal normal, tumor and metas-
- tasis tissues and bioinformatic modeling of miRNA-1 therapeutic applications. *PLoS One* 8, e67461.
- Rosenberg, S.A., and Restifo, N.P. (2015). Adoptive cell transfer as personalized immunotherapy for human cancer. *Science* 348, 62–68.
- Rusinova, I., Forster, S., Yu, S., Kannan, A., Masse, M., Cumming, H., Chapman, R., and Hertzog, P.J. (2013). Interferome v2.0: an updated database of annotated interferon-regulated genes. *Nucleic Acids Res.* 41, D1040–D1046.
- Santini, S.M., Lapenta, C., Santodonato, L., D'Agostino, G., Belardelli, F., and Ferrantini, M. (2009). IFN-alpha in the generation of dendritic cells for cancer immunotherapy. *Handb. Exp. Pharmacol.* 295–317.
- Sarantopoulos, J., Shapiro, G.I., Cohen, R.B., Clark, J.W., Kauh, J.S., Weiss, G.J., Cleary, J.M., Mahalingam, D., Pickard, M.D., Faessel, H.M., et al. (2015). Phase I study of the investigational NEDD8-activating enzyme inhibitor Pevonedistat (TAK-924/MLN4924) in patients with advanced solid tumors. *Clin. Cancer Res.* 22, 847–857.
- Sharma, P., and Allison, J.P. (2015). The future of immune checkpoint therapy. *Science* 348, 56–61.
- Sistigu, A., Yamazaki, T., Vacchelli, E., Chaba, K., Enot, D.P., Adam, J., Vitale, I., Goubar, A., Baracco, E.E., Remedios, C., et al. (2014). Cancer cell-autonomous contribution of type I interferon signaling to the efficacy of chemotherapy. *Nat. Med.* 20, 1301–1309.
- Stewart, C.A., Metheny, H., Iida, N., Smith, L., Hanson, M., Steinhagen, F., Leighty, R.M., Roers, A., Karp, C.L., Muller, W., and Trinchieri, G. (2013). Interferon-dependent IL-10 production by Tregs limits tumor Th17 inflammation. *J. Clin. Invest.* 123, 4859–4874.
- Talmadge, J.E., Donkor, M., and Scholar, E. (2007). Inflammatory cell infiltration of tumors: Jekyll or Hyde. *Cancer Metastasis Rev.* 26, 373–400.
- Topalian, S.L., Hodi, F.S., Brahmer, J.R., Gettinger, S.N., Smith, D.C., McDermott, D.F., Powderly, J.D., Carvajal, R.D., Sosman, J.A., Atkins, M.B., et al. (2012). Safety, activity, and immune correlates of anti-PD-1 antibody in cancer. *N. Engl. J. Med.* 366, 2443–2454.
- Trinchieri, G. (2010). Type I interferon: friend or foe? *J. Exp. Med.* 207, 2053–2063.
- Uze, G., Schreiber, G., Piehler, J., and Pellegrini, S. (2007). The receptor of the type I interferon family. *Curr. Top. Microbiol. Immunol.* 316, 71–95.
- Wang, Y., Swiecki, M., Celli, M., Alber, G., Schreiber, R.D., Gilfillan, S., and Colonna, M. (2012). Timing and magnitude of type I interferon responses by distinct sensors impact CD8 T cell exhaustion and chronic viral infection. *Cell Host Microbe* 11, 631–642.
- Wang, L.C., Lo, A., Scholler, J., Sun, J., Majumdar, R.S., Kapoor, V., Antzis, M., Cotner, C.E., Johnson, L.A., Durham, A.C., et al. (2014). Targeting fibroblast activation protein in tumor stroma with chimeric antigen receptor T cells can inhibit tumor growth and augment host immunity without severe toxicity. *Cancer Immunol. Res.* 2, 154–166.
- Xu, H.C., Grusdat, M., Pandya, A.A., Polz, R., Huang, J., Sharma, P., Deenen, R., Kohrer, K., Rahbar, R., Diefenbach, A., et al. (2014). Type I interferon protects antiviral CD8+ T cells from NK cell cytotoxicity. *Immunity* 40, 949–960.
- Zhao, Z., Condomines, M., van der Stegen, S.J., Perna, F., Kloss, C.C., Gunset, G., Plotkin, J., and Sadelain, M. (2015). Structural design of engineered costimulation determines tumor rejection kinetics and persistence of CAR T cells. *Cancer Cell* 28, 415–428.
- Zheng, H., Qian, J., Carbone, C.J., Leu, N.A., Baker, D.P., and Fuchs, S.Y. (2011). Vascular endothelial growth factor-induced elimination of the type I interferon receptor is required for efficient angiogenesis. *Blood* 118, 4003–4006.
- Zhou, P., Shaffer, D.R., Alvarez Arias, D.A., Nakazaki, Y., Pos, W., Torres, A.J., Cremasco, V., Dougan, S.K., Cowley, G.S., Elpek, K., et al. (2014). In vivo discovery of immunotherapy targets in the tumour microenvironment. *Nature* 506, 52–57.
- Zitvogel, L., Galluzzi, L., Kepp, O., Smyth, M.J., and Kroemer, G. (2015). Type I interferons in anticancer immunity. *Nat. Rev. Immunol.* 15, 405–414.

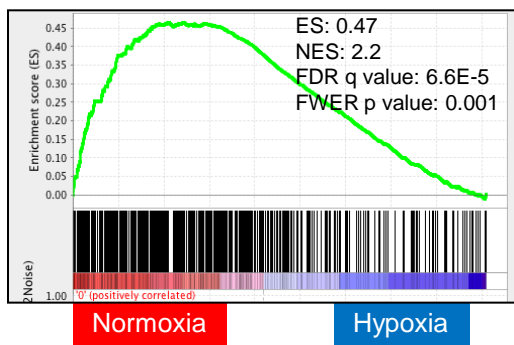
Supplemental Information

Inactivation of Interferon Receptor Promotes the Establishment of Immune Privileged Tumor Microenvironment

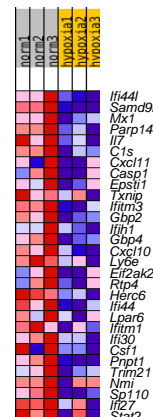
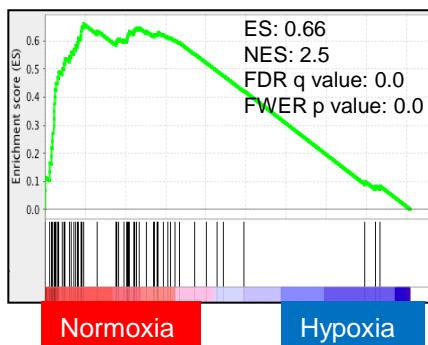
Kanstantsin V. Katlinski, Jun Gui, Yuliya V. Katlinskaya, Angelica Ortiz, Riddhita Chakraborty, Sabyasachi Bhattacharya, Christopher J. Carbone, Daniel P. Beiting, Melanie A. Girondo, Amy R. Peck, Ellen Puré, Priya Chatterji, Anil K. Rustgi, J. Alan Diehl, Constantinos Koumenis, Hallgeir Rui, and Serge Y. Fuchs

Supplemental Data

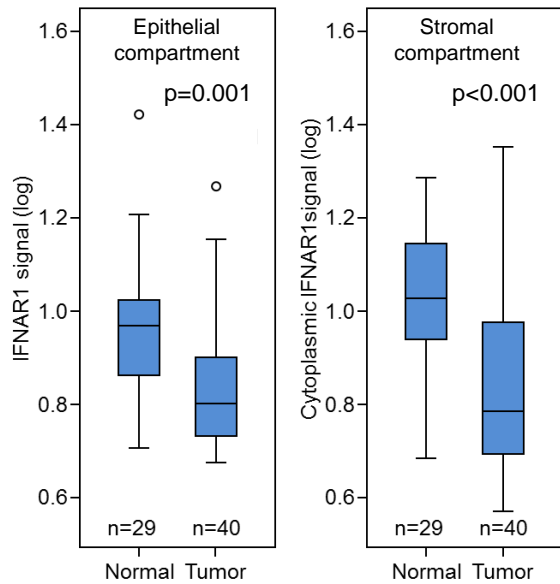
A



B



C



D

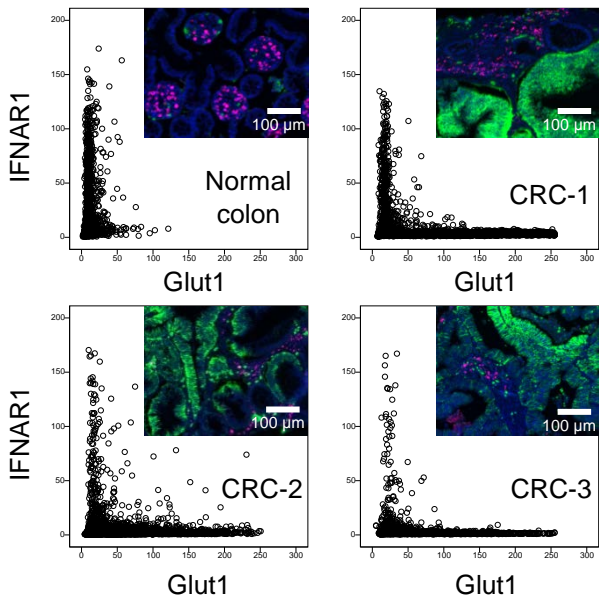


Figure S1 (related to Figure 1). Status of IFN and immune pathways in tumor microenvironment.

(A) Analysis of gene array data on expression of genes downregulated in the hypoxic areas of transplanted rat 9L glioma tumors (reported in (Marotta et al., 2011)). GSEA results for the immune pathway are shown. **(B)** Gene Set Enrichment Analysis (GSEA) (left panel) and heat map (right panel) of IFN signaling pathway genes profiled from the normoxic and hypoxic tumor areas. **(C)** Quantification of immunohistochemical analysis of IFNAR1 protein levels in epithelial and stromal compartments of normal colon and colorectal adenocarcinoma from samples from the University of Pennsylvania's tissue microarray (described in (King et al., 2011)). Box plot showing nuclear IFNAR1 levels in representative normal and cancer cases indicates median (dark line), 25-75% range (box), minimum and maximum values (whiskers) and individual scatter plot values (circles) overlaying the box plot. **(D)** Analysis of IFNAR1 and tumor microenvironment stress marker, GLUT1-positive cells in normal colon and colorectal tumors. A panel of 54 colorectal adenocarcinomas and 30 normal colon specimens were co-stained for GLUT1 (green) and IFNAR1 (red). The representative images of normal colon and three CRC samples as well as the scatterplots of quantitative IHC values are shown. Image quantification was performed using Tissue Studio. Scale bars: 100 μ m.

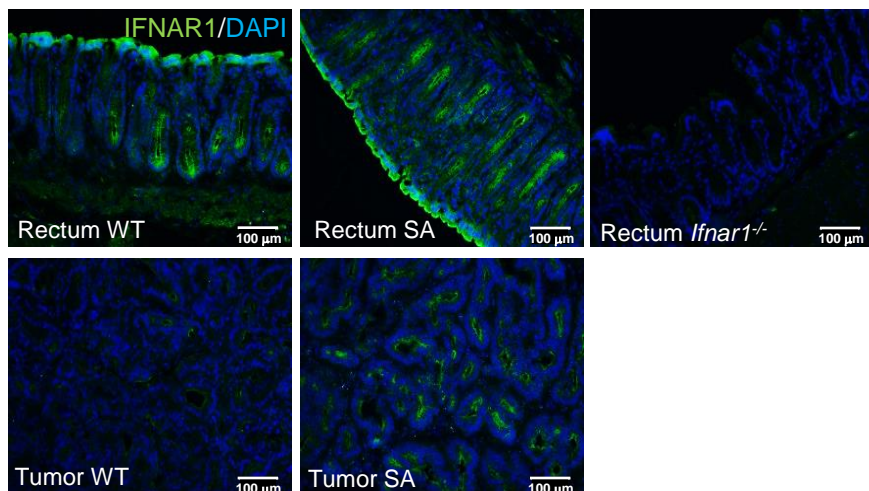
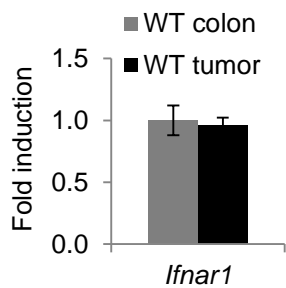
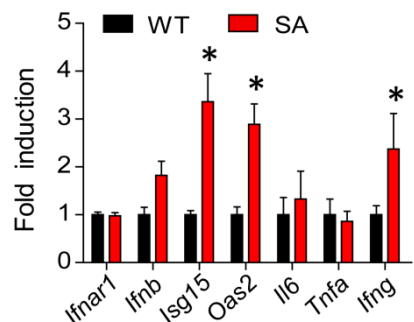
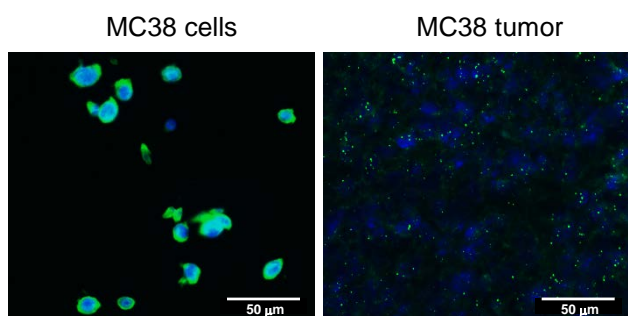
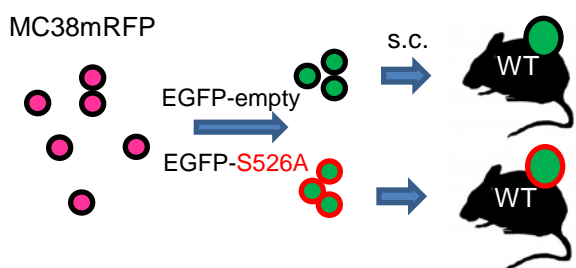
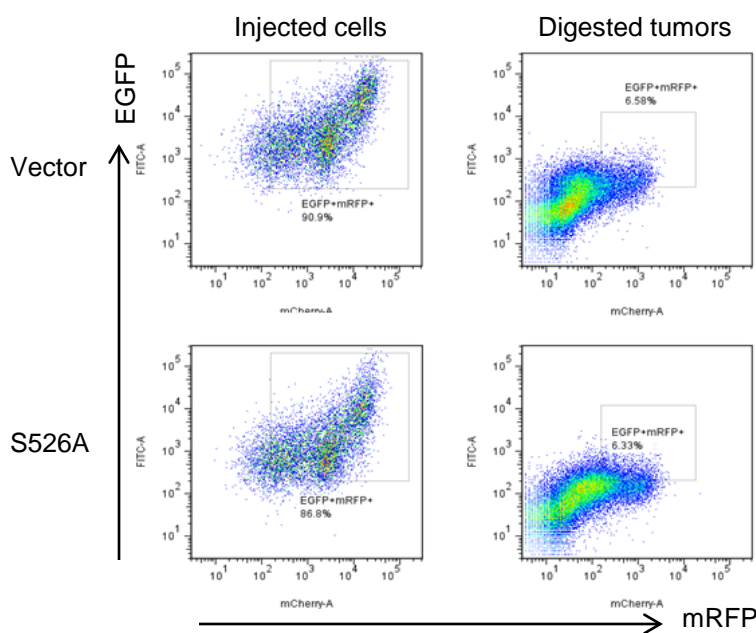
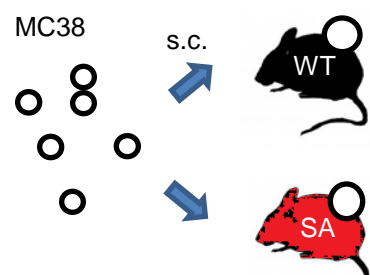
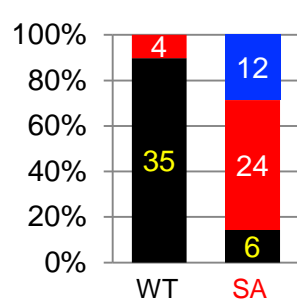
A**B****C****D****E****F****G****H**

Figure S2 (related to Figure 2). Role of downregulation of IFNAR1 in the stromal compartment in colorectal carcinogenesis and growth of transplanted adenocarcinomas.

(A) Representative immunofluorescent analysis of IFNAR1 levels (green) in rectums from WT (upper left), SA (upper middle), and *Ifnar1*^{-/-} (upper right – serves as a negative control) mice and rectal tumors from AOM-DSS-treated WT (lower left) and SA (lower right) mice. Here and thereafter, the sections were counterstained with DAPI (blue). Scale bar: 100 µm. **(B)** qPCR analysis of *Ifnar1* mRNA expression in tumors and benign tissues from AOM-DSS-treated mice. Mean values (the group of 3 mice)±SEM are shown. **(C)** qPCR analysis of mRNA for indicated genes in AOM-DSS-induced tumors from WT and SA mice. Mean values (8 tumors from the group of 5 mice)±SEM are shown. Here and thereafter: * p<0.05; ** p<0.01; *** p<0.001. **(D)** Immunofluorescent analysis of IFNAR1 levels (green) on MC38-derived tumors compared to cultured MC38 cancer cells. Samples were contrasted with DAPI (blue). Scale bar: 50 µm; **(E)** Design of experiments restoring IFNAR1 levels in cancer cells. MC38mRFP cells were transduced with pCIG-EGFP or pCIG-IFNAR1^{S526A}-EGFP constructs and GFP-positive tumor cells were injected into the flank of syngeneic WT mice (1×10^6 per mouse). **(F)** FACS analysis of MC38mRFP cells transduced with pCIG-EGFP or pCIG-IFNAR1^{S526A}-EGFP constructs was carried out either in cells immediately prior to injection into animals (“Injected cells”) or in cells obtained from resulting tumors upon their digestion with collagenase (“Digested tumors”). MC38mRFP and MC38 parental cells were used as controls for gating on GFP/mRFP positive cells. **(G)** Design of experiments restoring IFNAR1 levels in the stroma. **(H)** Combined data depicting the outcome of MC38 tumor growth in WT and SA are shown. Tumors smaller than median tumor size in WT minus 2σ (SD) at day 32 were considered as delayed.

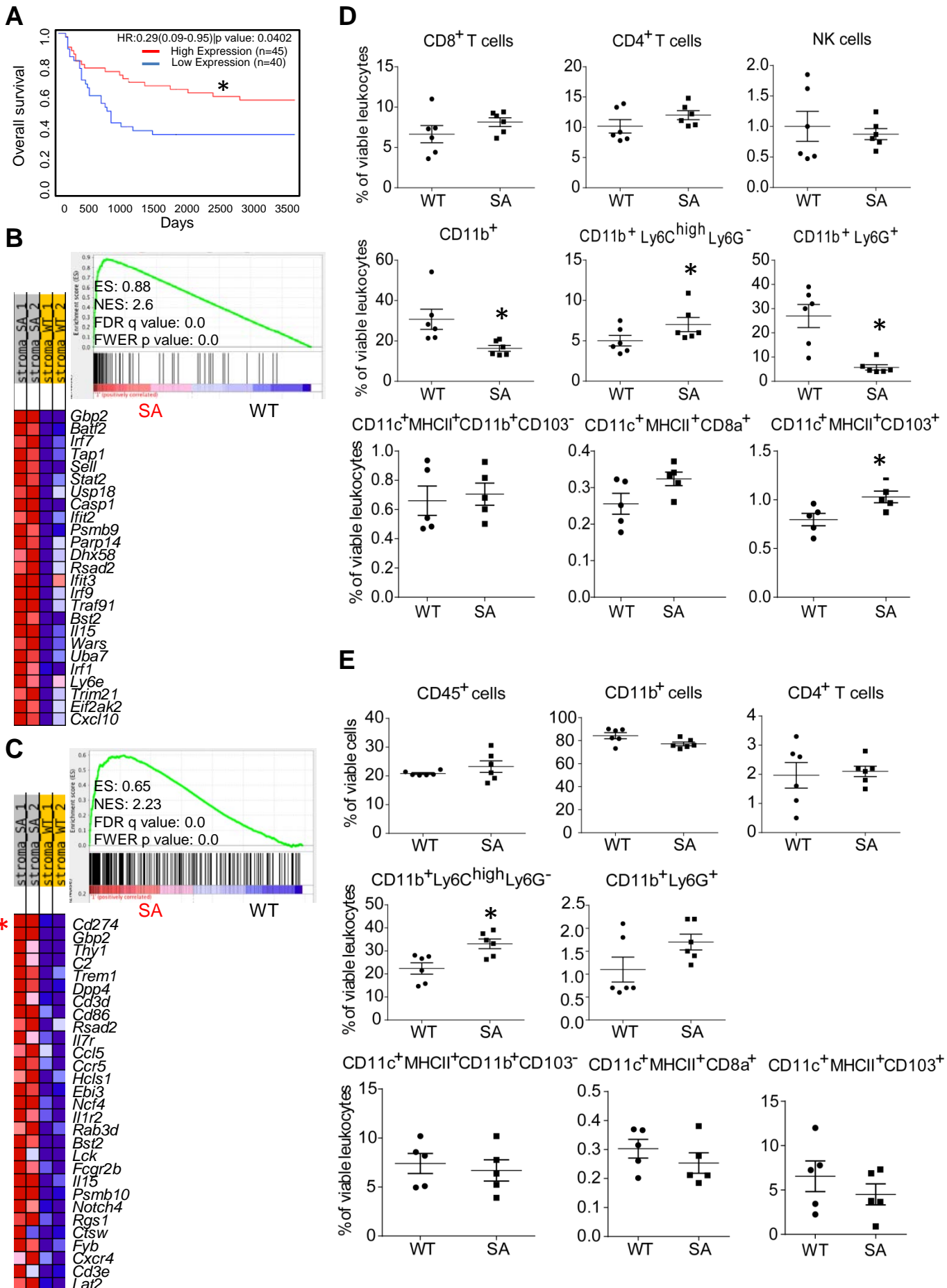


Figure S3 (related to Figure 3). Gene expression associated with IFNAR1 downregulation and prognosis in CRC patients.

(A) Survival of adjusted for the stage CRC patients (GSE30378) harboring expression pattern of 30 selected genes (Table S1) similar to MC38 that grew either in WT (blue) or in SA (red) mice **(B)** GSEA results and heat map of IFN α / β signaling pathway genes of the transcriptome profiles of enriched stromal (mRFP negative) cells sorted from MC38mRFP tumors harvested at day 21 (time point A1) and used for RNA isolation and microarray analysis. **(C)** GSEA results and heat map of immune system genes described in panel B. Asterisk denotes the most dramatically altered *Cd274* gene expression. **(D)** Percentage of splenic leukocyte populations in MC38 tumor bearing animals. Cell populations were defined as follows: CD4 $^{+}$ T cells (CD11b $^{-}$ CD11c $^{-}$ NK1.1 $^{-}$ CD3 $^{+}$ CD4 $^{+}$), CD8 $^{+}$ T cells (CD11b $^{-}$ CD11c $^{-}$ NK1.1 $^{-}$ CD3 $^{+}$ CD8 $^{+}$), NK cells (CD3 $^{-}$ NK1.1 $^{+}$). **(E)** Percentage of infiltrating leukocytes in MC38 tumors grown in WT and SA mice after s.c. injection of 1x10 6 MC38 cells (as in panel D). Tumors were excised at the size of 200-300 mm 2 and digested with collagenase to prepare single cell suspensions.

Data shown as Mean \pm SD (n = 5-6).

Table S1 (related to Figure 3). The list of 30 genes upregulated in the enriched stromal compartment (mRFP-negative cells) from SA MC38mRFP tumors compared to WT MC38mRFP tumors (harvested at the A0 time point in experiment as described in Figure 3A).

<i>Nup210</i>	nucleoporin 210kDa
<i>Irf7</i>	interferon regulatory factor 1
<i>Cd69</i>	CD69 molecule
<i>Ifit2</i>	interferon-induced protein with tetratricopeptide repeats 2
<i>Daxx</i>	Death domain-associated protein 6
<i>Il10ra</i>	IL10RA interleukin 10 receptor, alpha
<i>Mx2</i>	MX dynamin-like GTPase 2
<i>Usp18</i>	ubiquitin specific peptidase 18
<i>Sh2d2a</i>	SH2 domain containing 2A
<i>Ass1</i>	argininosuccinate synthase 1
<i>Hpx</i>	hemopexin
<i>Clec7a</i>	C-type lectin domain family 7, member A
<i>Lcn2</i>	lipocalin 2
<i>Cd40</i>	TNF receptor superfamily member 5
<i>Csf2ra</i>	colony stimulating factor 2 receptor, alpha, low-affinity (granulocyte-macrophage)
<i>Cxcl9</i>	chemokine (C-X-C motif) ligand 9
<i>Ccl17</i>	chemokine (C-C motif) ligand 17
<i>Slc7a8</i>	solute carrier family 7 (amino acid transporter light chain, L system), member 8
<i>Cd86</i>	CD86 molecule
<i>Tlr4</i>	toll-like receptor 2
<i>Sema4a</i>	sema domain, immunoglobulin domain (Ig), transmembrane domain (TM) and short cytoplasmic domain, (semaphorin) 4A
<i>Sdc3</i>	syndecan 3
<i>Cd83</i>	CD83 molecule
<i>Cytip</i>	cytohesin 1 interacting protein
<i>Oas3</i>	2'-5' oligoadenylate synthetase 3
<i>Tiam1</i>	T-cell lymphoma invasion and metastasis 1
<i>Il1rn</i>	interleukin 1 receptor antagonist
<i>Cxcl10</i>	chemokine (C-X-C motif) ligand 10
<i>Aim1</i>	absent in melanoma 1
<i>Stat4</i>	signal transducer and activator of transcription 4

A

- WT DC+SIINFEKL+OT1 T-cells
- SA DC+SIINFEKL+OT1 T-cells
- WT DC+OT1 T-cells
- SA DC+OT-1 T-cells

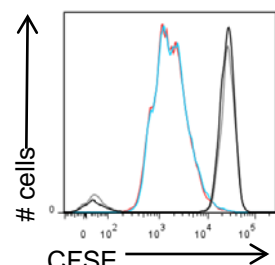
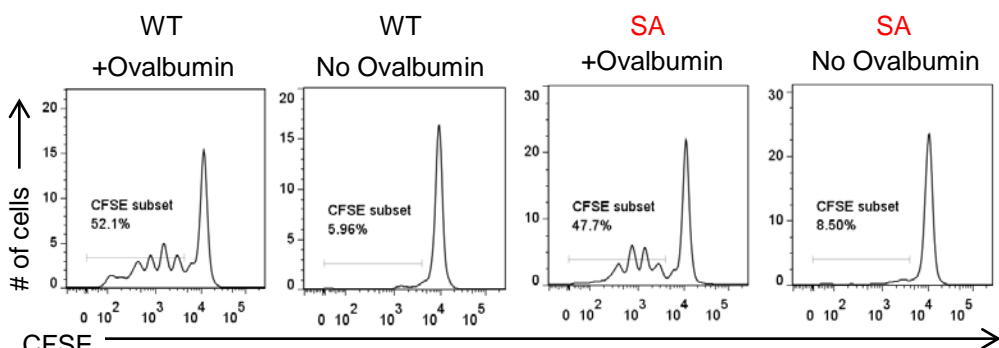
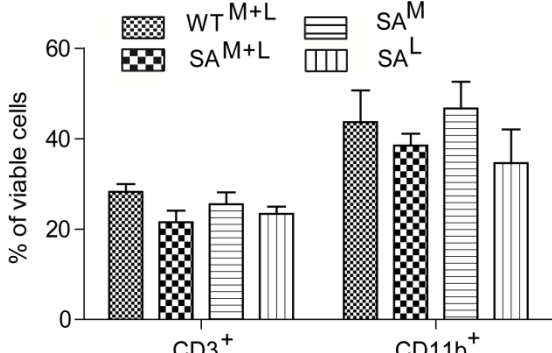
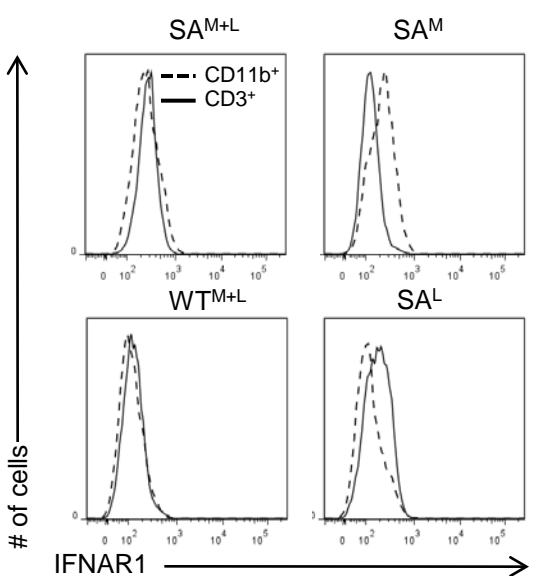
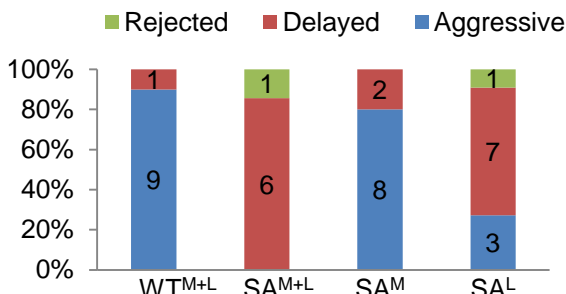
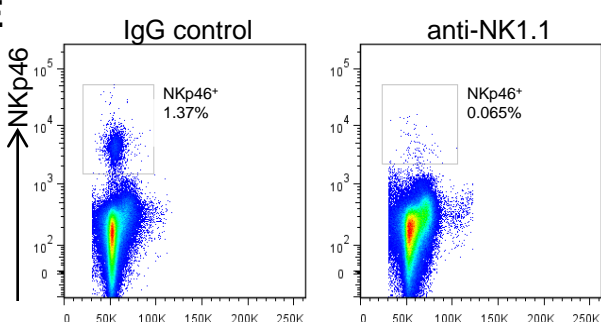
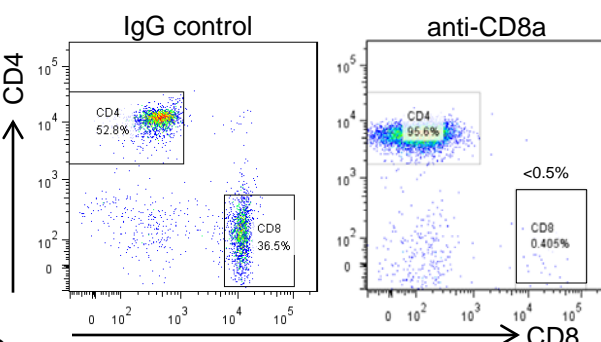
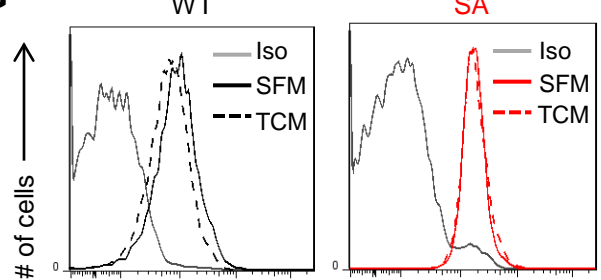
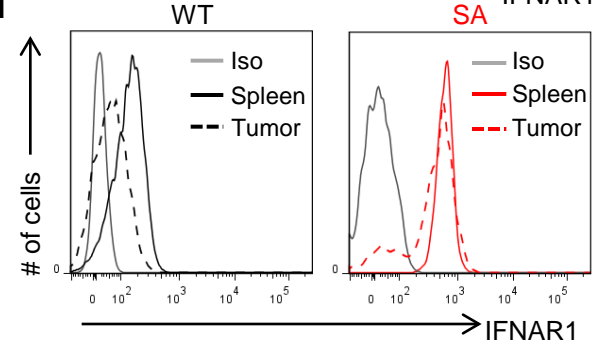
**B****C****D****E****F****G****H**

Figure S4 (related to Figure 4). Downregulation of IFNAR1 in cytotoxic T lymphocytes and immunosuppressive tumor microenvironment in CRC.

(A) Representative flow cytometry analysis of proliferation of CFSE-labeled OT-1 CD3⁺CD8⁺ T cells stimulated with CD11c⁺ splenic WT and SA dendritic cells loaded with SIINFEKL peptide. Dilution of the cell proliferation dye (CFSE) was measured 60 hr later. Data are representative of two independent experiments. **(B)** Representative flow cytometry analysis of proliferation of CFSE-labeled CD3⁺CD8⁺ OT-1 WT T cells in response to ovalbumin cross-presented by WT or SA CD11c⁺ dendritic cells. CD11c⁺ cells were isolated from the spleens of WT or SA mice and co-cultured with irradiated, ovalbumin-loaded (left panels) or unloaded (right panels) MHC class I mismatched splenocytes and CFSE-labeled OT-1 T cells. After 72 hr incubation, proliferation of OT-1 T cells was determined by CSFE dilution. Histograms represent CFSE levels in the CD8⁺ T cells. Data are representative of at least two independent experiments that yielded similar results. **(C)** Representative histograms of cell surface IFNAR1 levels on myeloid and lymphoid cells (upper panels) and the percentage of these cells in the spleens from indicated bone marrow chimeras (lower panel) at the end of experiment shown in Figure 4D. Data are shown as Mean \pm SEM (n=4-6). **(D)** Outcome of MC38 tumor growth in mixed bone marrow chimeras. Tumors smaller than median tumor size in WT^{M+L} minus 2 σ (SD) at day 32 were considered as delayed. **(E)** Percentage of NKp46⁺ NK cells in the spleens of tumor bearing mice treated with IgG control or anti-NK.1.1 antibodies at the end of experiment. **(F)** Percentage of CD3⁺CD8⁺ cells in the spleens of tumor bearing mice treated with anti-CD8a antibodies at the end of the experiment. **(G)** Representative histograms of cell surface IFNAR1 levels on CD8⁺ T cells isolated from spleens of WT or SA mice and incubated for 2 hr in the presence of serum-free media (SFM) or media conditioned by MC38 tumor cells (TCM). **(H)** Representative histograms of cell surface IFNAR1 levels on CD3⁺CD8⁺ cells isolated from spleens or MC38 tumors from WT (left panel) or SA (right panel) tumor-bearing mice.

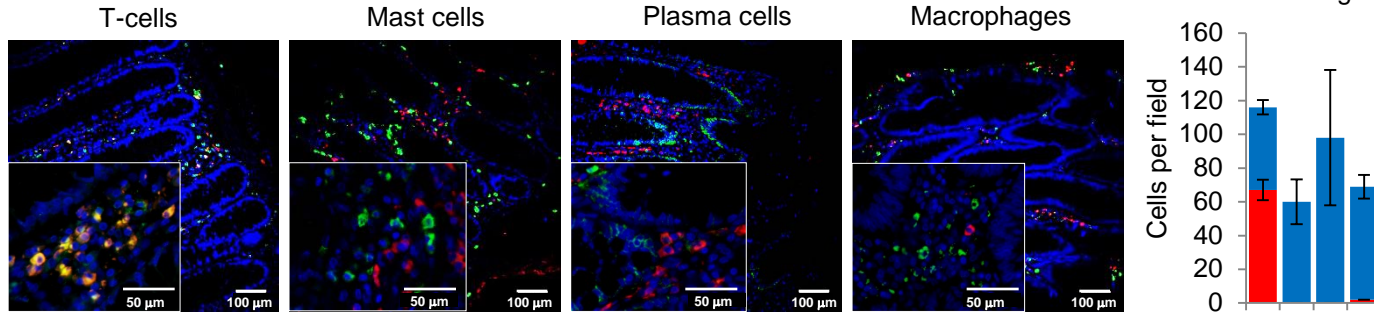
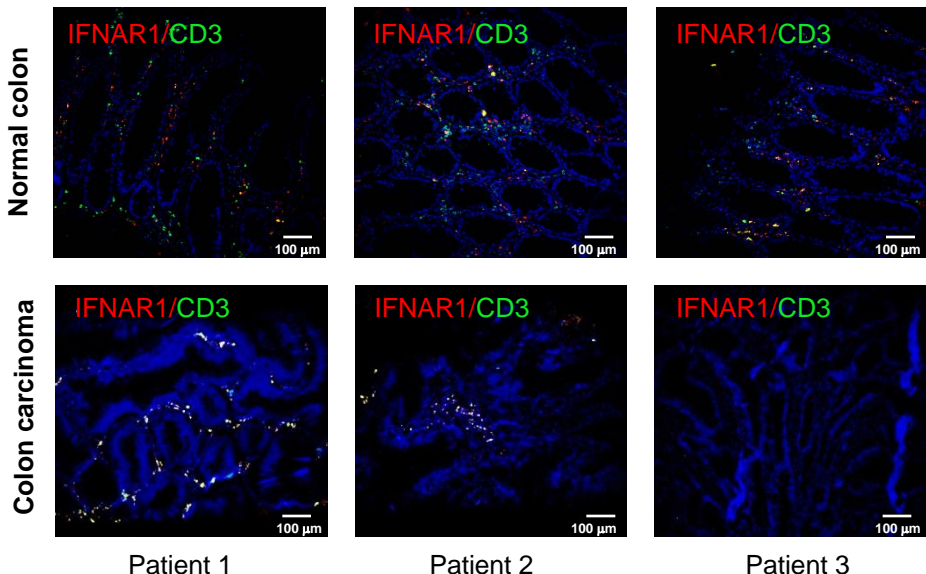
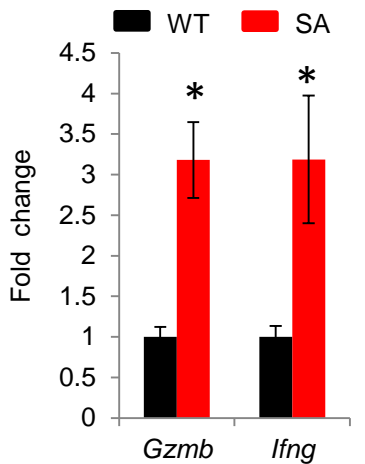
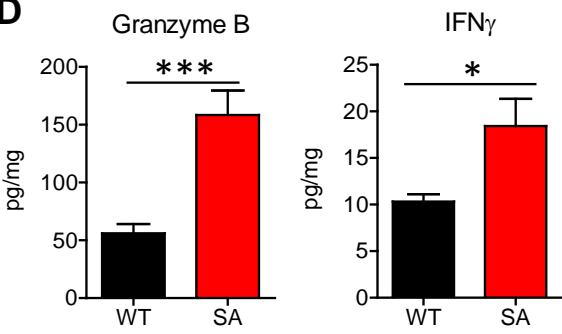
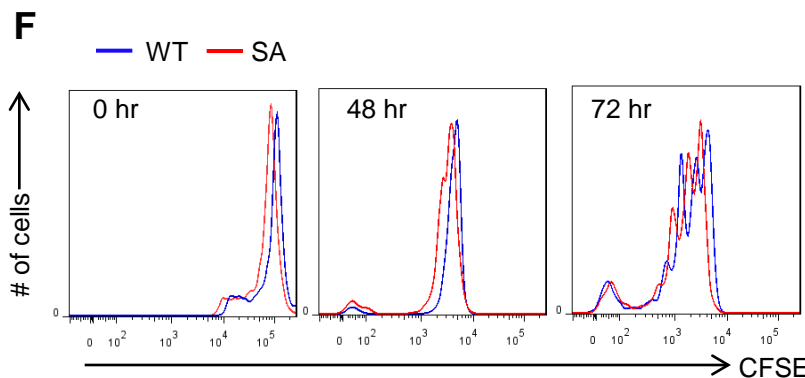
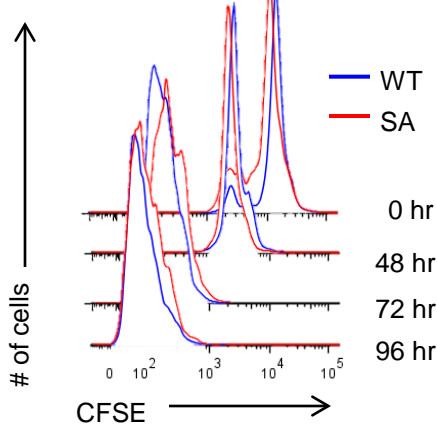
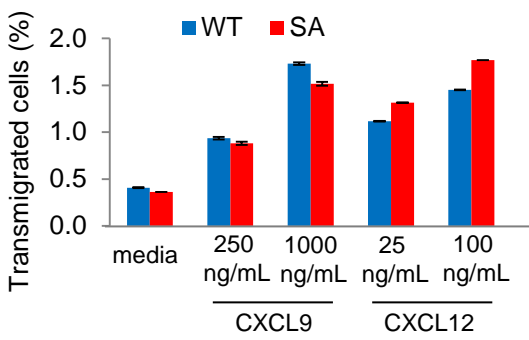
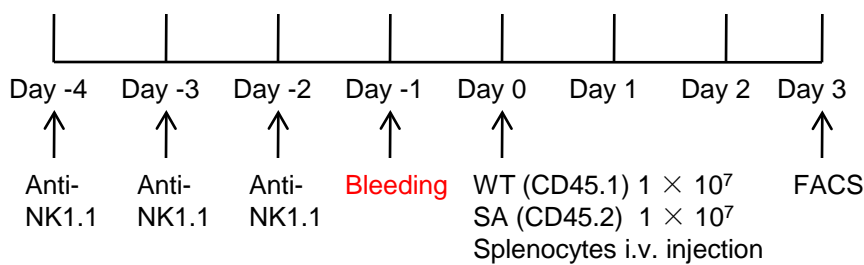
A**B****C****D****F****E****G**

Figure S5 (related to Figure 5). Role of IFNAR1 downregulation in survival/intra-tumoral accumulation of CTL.

(A) Representative immunofluorescent staining of normal human colon sections with antibodies against IFNAR1 (red, all panels) and indicated cell specific markers (green): anti-CD3 (pan T cells), anti-mast cell tryptase (mast cells), anti-CD138 (plasma cells), anti-CD68 (macrophages). Sections were contrasted with DAPI (blue). Scale bars: 100 μ m. Inserts with a higher magnification are shown in the bottom left corner of each image (scale bars 50 μ m). Quantification of IFNAR1^{high} and IFNAR1^{low} cells (from at least 20 random fields) is shown on the right. **(B)** Representative immunofluorescent analysis of CD3⁺ T cells infiltration of human CRC. Tumor sections stained with antibodies against IFNAR1 (red) and CD3 (green) and contrasted with DAPI (blue). **(C)** Real time PCR analysis of mRNA of indicated genes in MC38 tumors grown in WT and SA mice. Tumors were harvested at the size of 200-300 mm² and used for RNA isolation. Mean values \pm SEM (n= 6 tumors for each group) are shown. **(D)** Results of ELISA analysis of IFNy and granzyme B in the lysates from indicated tumors described in panel C. Mean values \pm SEM (n= 6 tumors for each group) are shown. **(E)** Proliferation of CFSE labeled OT-1 CD3⁺CD8⁺ WT and OT-1 CD3⁺CD8⁺ SA upon stimulation of splenocytes with SIINFEKL peptide. Dilution of CFSE was measured after indicated time periods. Data are representative of 2 independent experiments (each in triplicates). **(F)** Proliferation of CFSE labeled OT-1 CD3⁺CD8⁺ WT and OT-1 CD3⁺CD8⁺ SA T cells from spleens of MC38-OVA tumor bearing *Rag1*^{-/-} mice. *Rag1*^{-/-} mice were s.c. injected with MC38-OVA (bright, 2x10⁶/mouse). When the tumors reached ~100 mm² (around 20 days), each animal received 5x10⁶ CFSE labeled WT or SA OT-1 T cells (i.v.). Levels of CFSE in spleen-derived CD3⁺CD8⁺ cells were assessed at 0, 48 hr and 72 hr after adoptive transfer. Data are representative of 3 independent experiments (each in triplicates). **(G)** The percentage of transmigrated CD3/CD28-activated T cells from WT and SA mice in response to CXCL12 or CXCL9 in trans-well migration assay. Data represent Mean \pm SD of two independent experiments (each in triplicates).

A**B**

IgG control Anti-NK1.1

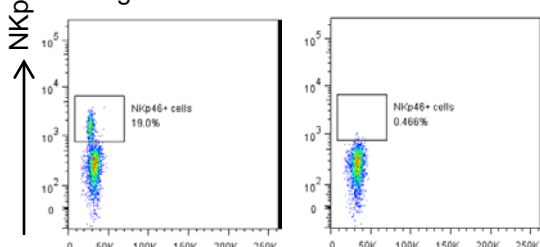
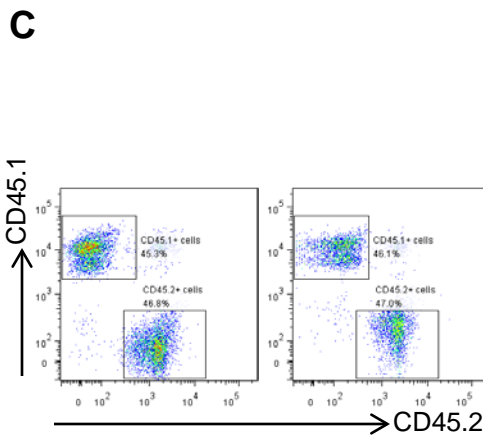
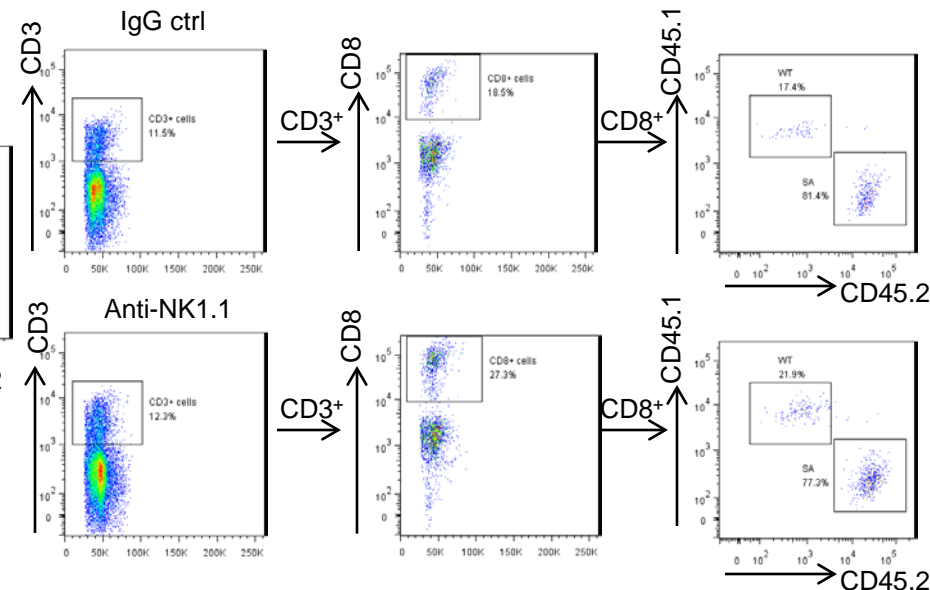
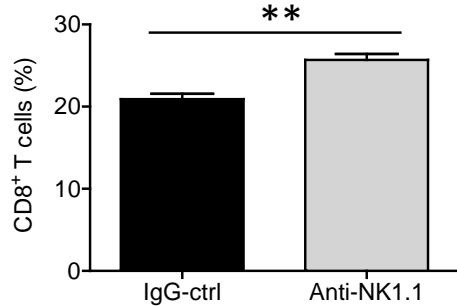
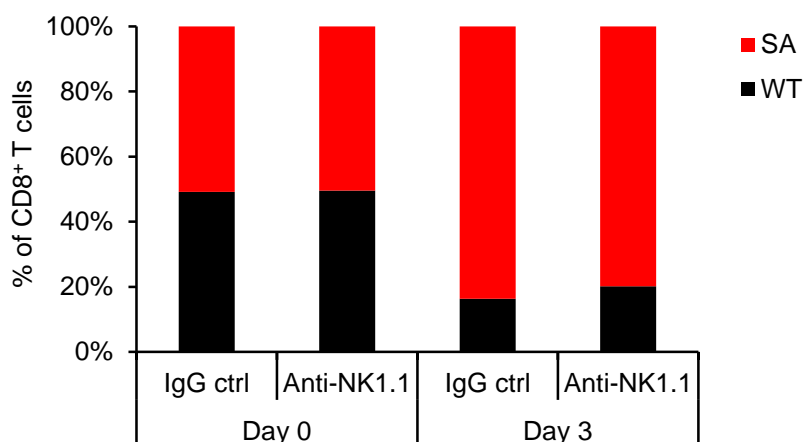
**C****D****E****F**

Figure S6 (related to Figure 6). Role of NK cells in the survival of WT or SA T cells.

Rag1 knockout mice were depleted (or not) of NK cells and viability of CD8⁺ T cells derived from the spleens from WT (CD45.1) or SA (CD45.2) co-injected into these mice in 1:1 ratio was assessed. **(A)** Schematic illustration for the experiment to determine the extent of NK-mediated killing of WT and SA T cells *in vivo*. **(B)** FACS analysis of the percentage of NKp46⁺ NK cells in the peripheral blood of *Rag1*^{-/-} mice treated with IgG control (left) or anti-NK1.1 (right) antibodies before cells injection. **(C)** FACS analysis of the composition of splenocytes mix (10⁷ cells from each WT (CD45.1) and SA (CD45.2) mice prior to injection into *Rag1*^{-/-} mice. **(D)** Representative of FACS analysis of composition of WT and SA CD8⁺ T cells in *Rag1*^{-/-} mice (treated with anti-NK1.1 or control antibody) three days after adoptive transfer. **(E)** Quantification of total CD8⁺T cells found in *Rag1*^{-/-} mice (as % of CD3⁺ cells) three days after adoptive transfer. **(F)** Quantification of the fraction of WT (CD45.1) and SA (CD45.2) CD8⁺ T cells in *Rag1*^{-/-} mice three days after adoptive transfer. NS, not significant.

Data are shown as Mean±SEM (n=5-6).

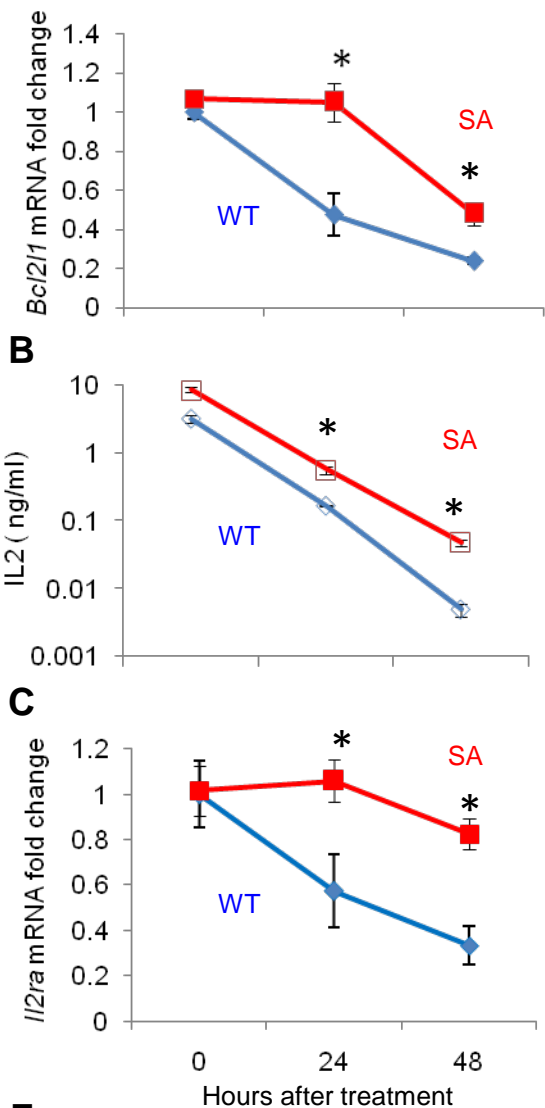
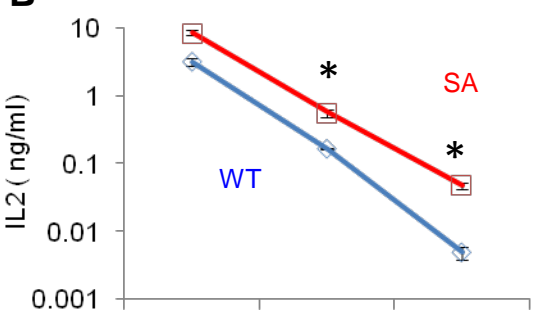
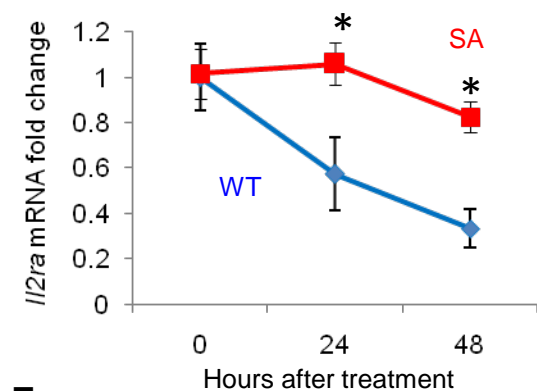
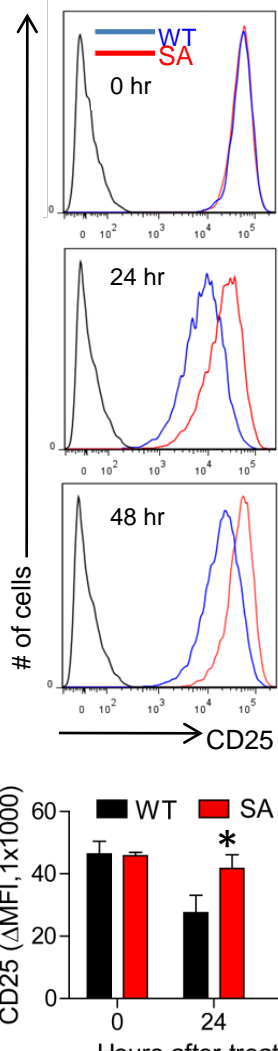
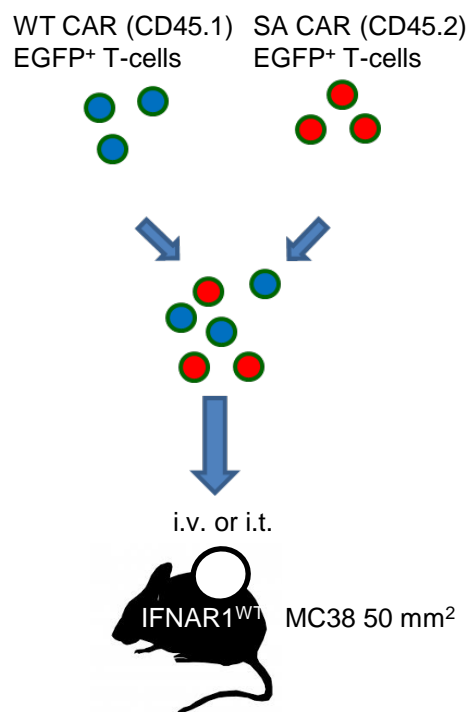
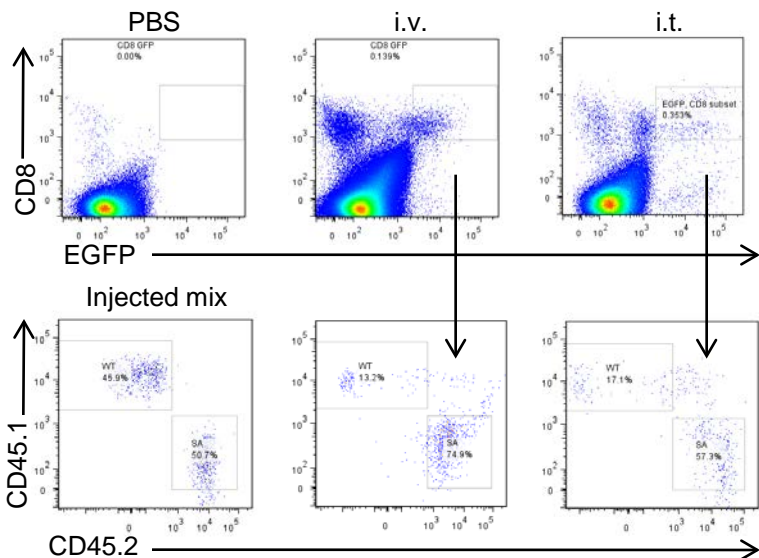
A**B****C****D****E****F**

Figure S7 (related to Figure 6). Role of downregulation of IFNAR1 on cytotoxic T lymphocytes in their survival within tumor microenvironment.

(A) Splenocytes from WT OT1 or SA OT1 mice were exposed to SIINFEKL peptide (0.5 µg/mL for 48 hr) and then cultured for indicated times and evaluated for viability and expression of apoptotic regulators. RT-PCR analysis of *Bcl2l1* mRNA expression levels in activated splenocytes from WT and SA OT-1 mice. Data are shown as Mean±SD (n=3 for each of 3 independent experiments). **(B)** ELISA analysis of IL2 levels in the supernatants of activated splenocytes cultured as in panel A. Data are shown as Mean±SD (n=3 for each of 3 independent experiments). **(C)** RT-PCR analysis of mRNA levels of *Il2α* chain expression in the culture of splenocytes from WT and SA OT-1 mice activated as in panel A. Data are shown as Mean±SD (n=3 for each of 3 independent experiments). **(D)** Representative histograms of CD25 expression on CD3⁺CD8⁺ cells at indicated time points from the culture of activated splenocytes from WT and SA OT-1 mice as described in panel A. Data are shown as Mean±SD (n=3 for each of 3 independent experiments, bottom panel). **(E)** Schematic representation of experiment described in Panel F. **(F)** Representative flow cytometry analysis of the fraction of viable FAP-CAR EGFP⁺ WT (CD45.1) or FAP-CAR EGFP⁺ SA (CD45.2) CTLs in the MC38 tumors 72 hr after injection (1:1 ratio) intravenously (i.v.) or directly into the tumors (i.t.) of WT MC38 tumor bearing mice.

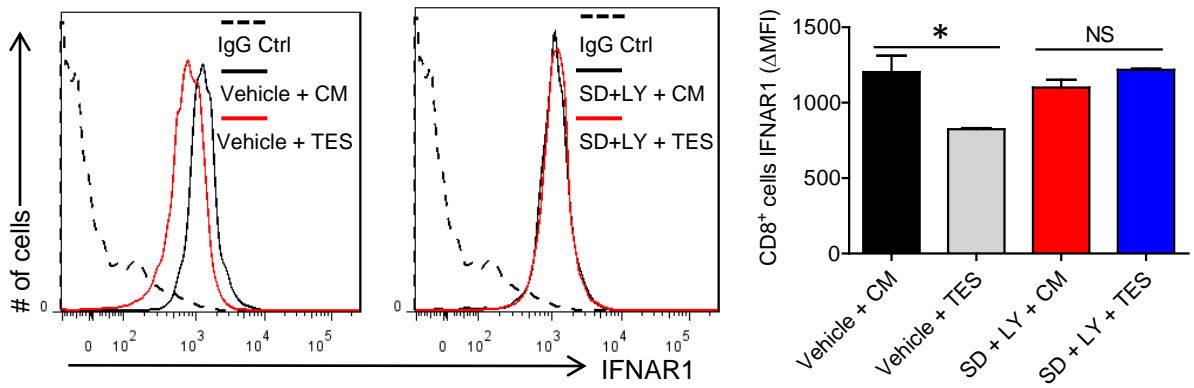
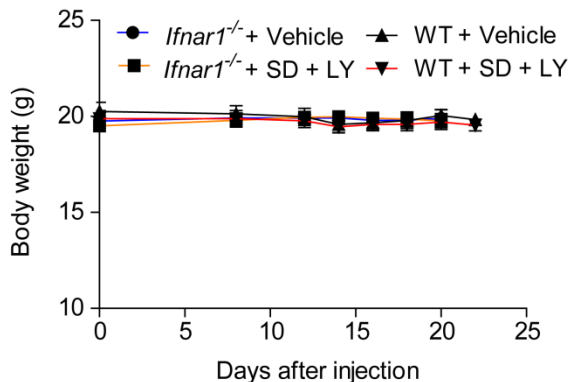
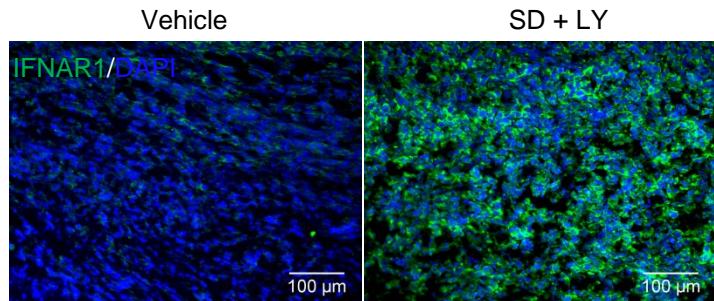
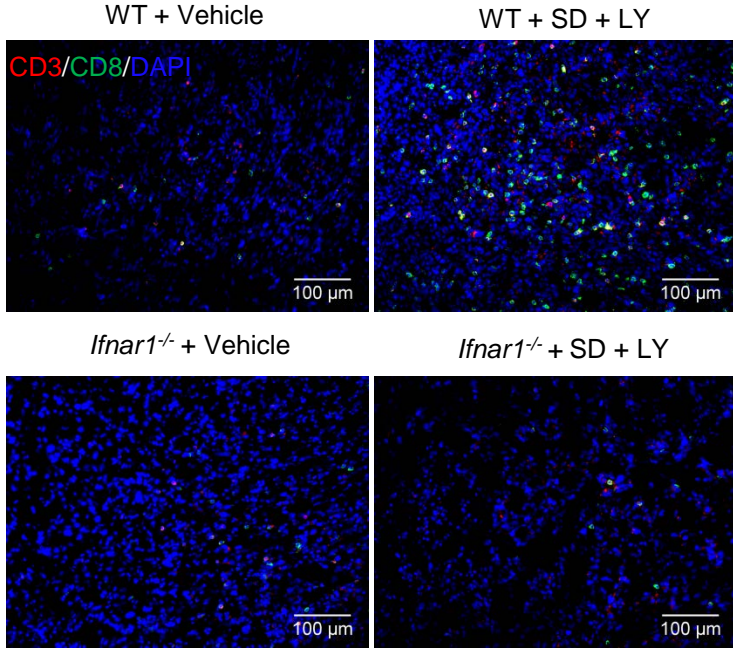
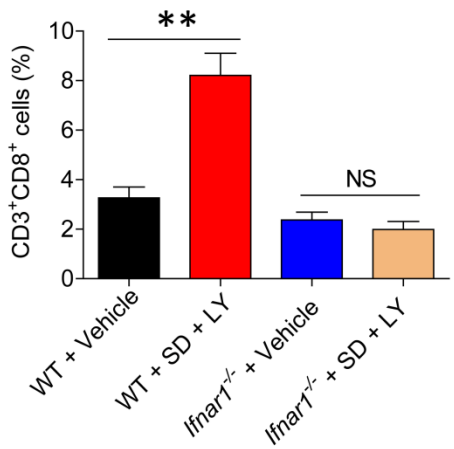
A**B****C****D****E**

Figure S8 (related to Figure 8). Effects of agents stabilizing IFNAR1 on the immune privileged niche.

(A) Cell surface IFNAR1 levels on WT CD3⁺CD8⁺splenocytes pre-treated with SD-208 PKD inhibitor (SD, 1 μ M) and LY2228820 p38 inhibitor (LY, 1 μ M) or vehicle (DMSO) for 2 hr and then treated with tumor explant supernatant (TES) or control media (CM) for additional 2 hr. A representative experiment and overall quantification (Mean \pm SEM from 3 independent experiments, each in triplicates) are shown. **(B)** Body weight of *Ifnar1*^{-/-} and WT mice treated with SD-208 PKD inhibitor (SD) and LY2228820 p38 inhibitor (LY) as described in Figure 8E and Materials and Methods. Data are shown as Mean \pm SEM (n=5 from each of 3 independent experiments). **(C)** Immunofluorescent analysis of IFNAR1 levels (green) in MC38 tumors grown in WT mice treated with vehicle (left panel) or PKD2 (SD) and p38 (LY) inhibitors (right panel) as described in Figure 8B-E. Samples were contrasted with DAPI (blue). Scale bars: 100 μ m. **(D)** Representative immunofluorescent analysis of CD3⁺CD8⁺ cells infiltration of MC38 tumors from Panel C. Tumor sections stained with indicated antibodies and contrasted with DAPI (blue). **(E)** Quantification of experiment described in Panel D. Scale bars: 100 μ m. Percent of CD3⁺CD8⁺cells among total DAPI-positive cells calculated as Mean \pm SEM from at least 20 random fields of 5 tumors for each treatment group is shown.

SUPPLEMENTAL EXPERIMENTAL PROCEDURES

Experiments in animals and statistical analysis.

All experiments with animals were carried out under the protocol 803995 approved by the IACUC of The University of Pennsylvania. All mice were on the C57Bl/6 background and had water ad libitum and were fed regular chow. *Rag1^{-/-}*, OT-1, *Ubc9-Cre^{ERT2}* and CD45.1 congenic mice were obtained from the Jackson Laboratory. Littermate C57BL/6 ("WT") and C57BL/6 *Ifnar1^{S526A}* mice ("SA") were described previously (Bhattacharya et al., 2014). *Mapk14^{f/f}* and *Ifnar1^{-/-}* mice were generously provided by Yibin Wang (UCLA) and Susan Weiss (University of Pennsylvania), respectively. Other strains were generated by intercrossing and the littermates of 6-8 weeks of age were used in the experiments. Mice were maintained in a specific pathogen-free facility in accordance with American Association for Laboratory Animal Science guidelines. Littermate animals from different cages were randomly assigned into the experimental groups, which were either co-housed or systematically exposed to other groups' bedding to ensure equal exposure to all group's microbiota.

All described results are representative of at least three independent experiments (n=5 mice per group in each experiment unless specified otherwise). All in vitro analyses using cells or tissues from each of these animals were done at least in biological triplicates (e.g. samples from 3 tumors, 3 spleens, etc). Data are presented as average ± S.E.M. Statistical analysis was performed using Microsoft Excel (Microsoft) or GraphPad Prism 7 software (GraphPad Prism Software Inc). Unpaired Student t test was used for the comparison between two groups. One-way ANOVA or two-way ANOVA analysis followed by the Bonferroni post-hoc test were used for the multiple comparisons. Repeated-measure two-way ANOVA (mixed-model) followed by the Bonferroni post-hoc test was used for the analysis of tumor growth curve. The Kaplan-Meier survival analysis is based on reaching the endpoint of tumor volume ~200 mm². A value of p <0.05 was considered significant.

Analysis of human cancers and statistical analysis

Use of pre-existing previously collected under informed consent human de-identified CRC tissue arrays and samples that could not be directly or indirectly linked to individual human subjects was exempt from the institutional review. Archived de-identified and de-coded, formalin-fixed, paraffin-embedded colorectal carcinomas and normal colon tissues in standard or CEMA tissue array format (LeBaron et al., 2005) were obtained from US Biomax, Inc (Derwood, MD; 242 adenocarcinomas with clinical outcome and matched adjacent normal tissue), and Thomas Jefferson University (54 adenocarcinomas and 30 normal epithelia (Wilson et al., 2014). Tissue array containing samples (40 adenocarcinomas and 20 normal epithelia) from an additional de-identified and coded cohort obtained from the University of Pennsylvania was previously described (King et al., 2011).

IFNAR1, phospho-tyrosine Stat2 (pTyr-Stat2) or GLUT1 were detected by chromogen or immunofluorescence IHC as previously described (Peck et al., 2011) with the following specifications: antigen retrieval with citric acid buffer (pH 6.0), rabbit polyclonal IFNAR1 antibody (Sigma, HPA018015; 1:200), rabbit polyclonal pTyr-Stat2 antibody (Sigma, SAB4503836; 1:400), mouse monoclonal GLUT1 (Thermo-Fisher, SPM498; 1:200), mouse monoclonal anti-pancytokeratin (clone AE1/AE3, DAKO, 1:100). Quantitative analysis was performed as previously described (Peck et al., 2016) using the ScanScope FL line scanner (Leica Biosystems) to capture high-resolution digital images followed by quantification of biomarker levels using Tissue Studio image analysis software (Definiens). Briefly, user-guided machine learning was performed to identify DAPI-stained cell nuclei and cytokeratin-stained cells within the epithelial or stromal regions of each tissue. Mean nuclear or cytoplasmic biomarker signal intensity then was calculated for epithelial and stromal regions. Differences in normal versus tumor specimens were compared by boxplot of log-transformed values and two-tailed t-test. Elements of the boxplot included median (dark line), 25-75 percentile (box), minimum and maximum values (whiskers) and scatter plot overlayed on the boxplot (each circle representing an individual data point).

For survival analysis, data-driven optimal cutpoint was determined by X-tile software (Camp et al., 2004) which dichotomized cases into high and low IFNAR1 categories. IBM SPSS Statistics 24 software was used for the survival analyses. Survival was analyzed using Kaplan-Meier survival curve estimator, log-rank test and Cox proportional hazards model.

Cell lines, culture conditions and viral infection. 293T and Phoenix cells (kindly provided by Z. Ronai, The Burnham Institute, San Diego, CA), MC38 colon adenocarcinoma cells (provided by S. Ostrand-Rosenberg, University of Maryland, Baltimore, MD), MC38OVAbright (Gilfillan et al., 2008), a gift from M. Smyth, Peter MacCallum Cancer Center), MC38mRFP cells (Powell et al., 2011), a gift from M. Wong, Oregon Health & Science University) were maintained at 37°C with 5% CO₂ in DMEM supplemented with 10% heat-inactivated FBS, penicillin, streptomycin and L-glutamine.

For lentiviral transduction, 293T cells were transfected with pCIG plasmids encoding enhanced green fluorescent protein (EGFP) or mouse ubiquitination deficient mutant IFNAR1^{S526A} together with EGFP (described in (Huangfu et al., 2012) using Lipofectamine Plus (Invitrogen). After 24-48 hr supernatants were passed through 0.45 µm nylon filter, mixed with Polybrene (8 µg/ml, Santa Cruz Biotech) and transferred to plated cancer cells. Transduction efficiency was verified by FACS analysis and usually was more than 80%. Flow-sorted GFP-positive cells were used for injections and tumor growth experiments described in Figures 2C and S2B-C.

Immunoprecipitation, immunoblotting and ELISA. Tumor samples or normal tissues were flash frozen and lysed by sonication. IFNAR1 was immunoprecipitated with anti-IFNAR1 antibodies (Leinco Technologies). Western blots were stained with rabbit anti-IFNAR1 antibodies (MyBioSource), anti-PKD2 (Bethyl Laboratories), anti-phospho-PKD2 (Abcam), anti-p38 (Santa Cruz Biotech), anti-phospho-p38 (Cell signaling) or anti-β-actin antibodies followed by anti-rabbit-HRP conjugated secondary antibodies (both from Sigma-Aldrich). ELISA-based assessment of levels of IFNy, Granzyme B and IL2 in tumor lysates or CTLs supernatants was carried out using appropriate kits (Cat# BMS609, eBioscience for IFNy; Cat# BMS6029, eBioscience for Granzyme B and Cat#431004, Biolegend for IL2).

Cancer cell transplantation and organ harvest. Cancer cells were inoculated subcutaneously in the right flank at 1x10⁶ cells (unless specified otherwise) in 100 µl Dulbecco-modified phosphate buffered saline (DPBS). Tumors were measured by caliper and size was calculated as (length × width). Mice were euthanized when the tumor reached 200-300 mm², organs were dissected, and single cell suspension was prepared from tumor tissue by digestion of 1- to 2-mm pieces with 1 mg/ml Collagenase D (Roche) and 100 µg/ml DNase I (Roche) in RPMI medium with 2% FBS for 1 hours with continuous agitation. Digestion mixture was passed through 70 µm cell strainer and washed with PBS supplemented with 2mM EDTA and 1% FBS. Single cells suspension from spleen was obtained by mechanical disruption. After erythrocyte lysis using red blood cell lysis buffer (RBC lysis buffer (155 mM NH₄Cl, 12 mM KHCO₃, and 0.1 mM EDTA) cells were used for immune staining. Intestinal epithelial cells (IECs) were isolated from the distal part of the colon by incubation of colon pieces in Hank's balanced salt solution containing 5 mM EDTA at 4 °C for 30 min.

Tumor explant supernatants (TES) were prepared from excised non-ulcerated tumors ~1.5 cm in diameter as described elsewhere (Ramakrishnan et al., 2014). Briefly, tumor tissues were bathed in 70% isopropanol for 30 seconds and then transferred to a Petri dish. Tumors were minced into pieces < 3 mm in diameter and digested in 2 mg/ml collagenase Type IV at 37°C for 1 hr. The digested tissue pieces were then pressed through a 70 µm cell strainer to create a single-cell suspension. Cells were washed with PBS and re-suspended in RPMI 1640 supplemented with 20 mM HEPES, 2 mM L-glutamine, 200 U/ml penicillin plus 50 mg/ml streptomycin, and 10% FBS. Cells were cultured for 24 hr at 10⁷ cells/ml, and the cell free supernatants were collected and kept at -80°C. The complete RPMI 1640 medium was control medium (CM).

Tumor conditioned media were prepared from cultured MC38 cells. Briefly, MC38 cells were cultured with DMEM supplemented with 10% FBS, 1% Penicillin/Streptomycin. When the cells were

80% confluent, the medium was replaced with serum-free medium. 48 hr later, the medium were collected and filtered with a 0.2 μ m filter, stored at -80°C until use.

AOM/DSS colorectal carcinogenesis. Co-housed experimental mice were intraperitoneally injected with 10 mg/kg azoxymethane (AOM; Sigma). A week later, they were supplied with tap water containing 2.5% dextran sodium sulfate (DSS, TdB Consultancy) for 7 days, followed by 14 days of regular water. This cycle was repeated three times and mice were sacrificed 2 weeks after the end of the last DSS cycle or at the end of 10 weeks. Colons were harvested, washed of feces with DPBS, and slit open longitudinally to count tumors. Tumors were flash frozen in liquid nitrogen or embedded into OCT media.

Flow cytometric analysis. Single-cell suspension was re-suspended in FACS buffer (PBS, 1% BSA) and blocked with anti-mouse CD16/32 antibodies and rat IgG for 10 min prior to staining with specific antibodies. Antibodies against cell surface markers: anti-CD3-FITC (APC, 145-2C11), anti-CD4-APC-Cy7 (RMA4-5), anti-CD8a-AF700 (PE, APC-Cy7, 53-6.7), anti-CD11b-PerCP-Cy5.5 (FITC, M1/70), anti-DX5-PE (DX5), anti-Gr-1-PE (RB6-8C5), anti-CD45-APC (FITC, 30-F11), anti-F4/80-APC (BM8), anti-CD11c-PE (PE-Cy7, FITC, N418), anti-NKp46-FITC (29A1.4), anti-NK1.1 PE-Cy7 (APC, PK136), anti-CD103 (BV 605TM, 2E7), anti-I-A/I-E-PE/Cy7 (MHC-II, M5/114.15.2), anti-H-2K^b-SIINFEKL (PE, 25-D1.16), anti-Ly6C-FITC (APC-Cy7, HK1.4), anti-Ly6G APC-Cy7 (PE, 1A8), anti-IFNAR1-PE (MAR1-5A3) were purchased from Biolegend. Samples were mixed with DAPI (1 ug/ml) and acquired on LSRIFortessa flow cytometer (BD Biosciences), and data were analyzed with FlowJo software (Tree Star).

Immunofluorescence and immunohistochemistry in mouse tissues. Cancer cells, tumors and organs harvested from mice were frozen in Tissue-Tek O.C.T. compound and cryosectioned in Leica CM3050 S Cryostats, fixed in acetone, washed and blocked with PBS containing 5% goat serum. Antibodies against cell surface markers: anti-CD3-biotin (145-2C11), anti-CD8a-AF488 (53-6.7) and streptavidin-dylight594 were purchased from Biolegend, antibody against IFNAR1 was from Sino Biological, Alexa Fluor 488 labeled goat antibodies against rabbit or rat IgG were from Life technologies. The sections were incubated with primary antibodies for 1 hr, washed and incubated with secondary Alexa Fluor 488 labeled goat antibodies for 1 hr. For double immune-staining sections were simultaneously stained with different primary Alexa Fluor 488-labeled and biotinylated antibodies followed by the incubation with streptavidin-dylight594. The sections were then washed and mounted with cover slip in ProLong gold antifade reagent containing 4',6-diamidino-2-phenylindole (DAPI). Immunofluorescent staining of human samples was performed on a Dako Autostainer. Antigen retrieval was performed using the DAKO PT-module with Tris/EDTA buffer (pH 9.0). Slides were coincubated with rabbit anti-pYSTAT2 (SAB4503836; Sigma-Aldrich) or anti-IFNAR1 (HPA018015; Sigma-Aldrich) and mouse anti-CD3 (F7.2.38; MDR), anti-CD138 (MI15; Biolegend), anti-CD68 (PGM1; Abcam), anti-Glut1 (SPM498; Abcam), anti-CD4 (1F6; Thermo), or anti-pancytokeratin (AE1/AE3; Dako). Slides were incubated with horseradish peroxidase-conjugated anti-mouse immunoglobulin G or Alexa-555-conjugated anti-rabbit immunoglobulin G secondary antibodies, followed by incubation with Cy5-tyramide (Perkin Elmer, Waltham, MA). Slides were coverslipped using DAPI-containing mounting media.

T cell proliferation analysis in vivo

Rag1^{-/-} mice were s.c. injected with MC38-OVA (bright) (2×10^6 /mouse). When the tumor size was reached to approximately 100 mm², mice received an intravenous transfer CFSE-labeled WT OT-1 T cells or SA OT-1 T cells (5×10^6 per mouse). At 48 hr and 72 hr after cells transfer, the splenocytes were isolated and CFSE level in CD3⁺CD8⁺ cells were analyzed by FACS.

NK killing assay in vivo

8 weeks Rag1^{-/-} mice were intraperitoneally injected daily with 100 μ g anti-NK1.1 antibody (Cat# 108712, Biolegend) or its IgG2a control antibody (Cat# 400281, Biolegend) for three days. After three days of injections, mice were bled to check the efficacy of NK cell depletion. Then WT (CD45.1) and SA (CD45.2) splenocytes were isolated and mixed in 1:1 ratio. The mixed splenocytes (total cell

number 2×10^7 in 200 μ l PBS for each mouse) were intravenously injected into the *Rag1*^{-/-} mice. Three days after cell transfer, splenocytes were isolated and the fraction of WT and SA CD3⁺CD8⁺ cells were analyzed by FACS.

Antibody and small molecules treatments. To deplete NK cells mice were intraperitoneally injected with 100 μ g of anti-NK1.1 antibodies (PK136, Biolegend) in 200 μ l of DPBS at day -2, 0, 7, 14, 21, 27 (relative to tumor injection). For CD8⁺ T cell depletion experiments, 200 μ g anti-CD8 (2.43; Bio-XCell) or control Ab (LTF-2; Bio-XCell) per mouse was delivered by i.p. injection at day -1, 0, 4, 8, 12, 16, 18, 22. For the PD-1 blockade experiment, 100 μ g anti-PD-1 (RMP1-14; Bio-XCell) or control Ab (2A3; Bio-XCell) was administered i.p. to mice every 4 days starting at day 8 for a total of six times. For IFNAR1 neutralizing experiments, the mice were injected with neutralizing IFNAR1 antibody (I-401, Leinco Tech) or IgG control antibody (I-536, Leinco Tech) at 1 mg/mouse (i.p. once a day; one injection for every five days starting on the next day after tumor cells inoculation).

To inhibit PKD and p38 kinases in vivo, MC38 tumor-bearing mice were treated by gavage with PKD inhibitor SD-208 (Selleckchem, 3mg/kg) and p38 inhibitor LY2228820 (Selleckchem, 1mg/kg) prepared in methylcellulose at the day 8, 9, 10, 12, 14, 16, 18, 20, and 22 after MC38 cells (1×10^6) inoculation. Gavage with analogous volumes of pure methylcellulose was used as a vehicle control procedure. For in vitro experiments, inhibitors were administered in DMSO at 1 μ M.

Bone marrow chimeras. Mixed bone marrow chimeric mice were obtained as described elsewhere (Diamond et al., 2011; Fuertes et al., 2011). Briefly, pooled tibial and femoral bone marrow cells from donor mice were lysed with RBC lysis buffer. To generate the “SA^L” mixed bone marrow chimeras, four parts of bone marrow from *Rag1*^{-/-} mice (WT *Ifnar1*) were mixed with one part of bone marrow from SA mice (*Ifnar1*^{SA}). To prepare the “SA^M” chimeras, 4 parts of bone marrow from SA *Rag1*^{-/-} mice were mixed with one part of bone marrow from WT mice. Control “SA^{M+L}” and “WT^{M+L}” chimeras were prepared by mixing four parts of bone marrow from SA *Rag1*^{-/-} or WT *Rag1*^{-/-} mice with 1 part of bone marrow from SA or WT mice, respectively. Resulting mixtures of indicated bone marrow cells injected retro-orbitally into recipient WT mice (10^7 cells per each recipient mouse) irradiated with a single dose of 9.5 Gy as described previously elsewhere (Diamond et al., 2011; Fuertes et al., 2011). Animals were maintained on trimethoprim-sulfamethoxazole (Hi-Tech Pharmacal) antibiotic water for 1 day prior and 2 weeks after irradiation, and tumor transplantation of chimeric mice was performed at least 8 weeks after reconstitution. Hematopoietic reconstitution of all animals was verified by flow cytometry of splenocytes at the end of the experiment. The levels of IFNAR1 on CD11b⁺ and CD3⁺ cells analyzed in tumor bearing mice at the end of experiments were used as a control for the expression of the *Ifnar1*^{SA} allele in specifically myeloid or lymphoid cell compartments (as shown in Supplemental Figure 4C).

Microarray analyses with Illumina whole-genome arrays. WT or SA mice were inoculated with MC38mRFP tumor cells and, upon tumor growth to volumes indicated in Figure 3A, tumors were excised and digested to produce the single-cell suspensions. Enriched total stromal (mRFP-negative) cells were obtained from flow sorting and used for gene expression profiling. Total RNA was isolated with miRNeasy mini kit (QIAGEN). Biotin-labeled cRNA preparations were obtained using TargetAmpTM-Nano Labeling Kit (Epicentre) as recommended by the manufacturer. Thereafter 0.75 μ g cRNA was hybridized to Illumina Sentrix Mouse-6 v.1 BeadChips, which were scanned with an Illumina BeadStation 500 (both from Applied Biosystems-Life Technologies Inc.). Data were collected with Illumina BeadStudio 3.1.1.0 software, and statistical analyses were conducted on the IlluminaGUI R-package. Gene sets from microarray data were analyzed for overlap with curated data sets (C5, H) in MSigDB using the web interface available at <http://www.broadinstitute.org/gsea/msigdb/index.jsp>. The raw data have been deposited to NCBI (accession number GSE76889). Prognostic value of the 30 gene signature that separates early SA tumor from early WT tumors was tested using the PROGgene2 software (Goswami and Nakshatri, 2013) and published gene expression data (adjusted for stage) from two separate datasets GSE41258 and GSE30378 (Agesen et al., 2012; Sheffer et al., 2009).

Real-time RT-PCR. RNA was extracted using TRIzol (Invitrogen, Carlsbad, CA, USA) and cDNA was prepared using the High Capacity cDNA Reverse Transcription Kit (Life Technologies). Real-time PCR was performed using SYBR reagent (Applied Biosystems, Carlsbad, CA, USA). The expression of each gene was calculated based on the cycle threshold (CT), set within the linear range of DNA amplification. The relative expression was calculated by Ct method, with normalization of raw data to a housekeeping gene (β -actin). The following primer sequences were used:

Ifnar1 FW 5'-CGACCAAGTGTGAATTCTCTTAC , RV 5'- ATCAACCTCATTCCACGAAGAT; ;
Ifnb FW 5'-AGCTCCAAGAAAGGACGAACAT-3', RV 5'-GCCCTGTAGGTGAGGTTGATCT-3'; *Ifng* FW 5'-ATGAACGCTACACACTGCATC-3', RV 5'-CCATCCTTTGCCAGTCCTC-3'; *Isg15* FW 5'-GGAACGAAAGGGGCCACAGCA-3', RV 5'-CCTCCATGGGCCTCCCTCGA-3'; *Oas2* FW 5'-CCCTGTGAAGGAAGTGGCTA -3', RV 5'- CTGTTGGAAGCAGTCCATGA -3'; *Irf7* FW 5'-CCACACCCCCATCTCGA-3', RV 5'-CCTCCGAGCCCCAAACTC-3'; *Stat1* FW 5'-CGCGCATGCAACTGGCATATAACT-3', RV 5'-AAGCTCGAACCACTGTGACATCCT-3'; *Tnfa* FW 5'-CATCTTCTAAAATTGAGTGACAA, RV 5'-TGGGAGTAGACAAGGTACAACCC-3'; *Il6* FW 5'-GAGGATACCACCTCCAACAGACC-3', RV 5'-AAGTGCATCATCGTTGTTCATACA-3' ; *Gzmb* FW 5'-CCCCGATGATCTCCCCGCTTTG-3', RV 5'-TCTGACGCTGGACCTAGGCG-3'; *Bcl2l1* FW 5'-TGCATTGTTCCCGTAGAGATCCA-3', RV 5'-TCTGAATGACCACCTAGAGCCTT-3'; *Il2ra* FW 5'-AACACCACCGATTCTGGCT-3', RV 5'-GTGGGTTGTGGGAAGTCTGT-3'; *Ido1* FW 5'-CCCACACTGAGCACGGACGG-3', RV 5'-TTGCGGGGCAGCACCTTCG-3'; *Ly6c1* FW 5'-TTGTCTGAGAGGAACCCCTC-3', RV 5'-GCACTCCATAGCACTCGTAG-3'; *Cxcl9* FW 5'-ATTGTGTCTCAGAGATGGTCTAATG-3', RV 5'-TGAAATCCCCTGGTCTCGAAAG-3'; *Gbp2* FW 5'-GATCCACATGTCGGAACCCA-3', RV 5'-GGAAAAGCCTGTCCTCTTCCC-3', *Pdcd1lg* FW 5'-GACCAGCTTTGAAGGGAAATG-3', RV 5'-CTGGTTGATTTGCGGTATGG-3', *Actb* FW 5'-AGAGGGAAATCGTGCCTGAC-3', RV 5'-CAATAGTGTGACCTGGCCGT-3'.

T-cell cells isolation, CFSE staining, activation and adoptive transfer. Pan T cells and CD8⁺ T cells were purified from mouse spleens with naive T cell isolation kit from Stem Cell and naive CD8⁺ cell isolation kit from Miltenyi Biotec respectively. 1x10⁷ T cells were reconstituted in RPMI media, stained with 2.5 mM CFSE at room temperature for 5 min and washed with DPBS supplemented with 10% FBS. For antigen specific activation of CD3⁺CD8⁺ cells, splenocytes from OT-1 WT and SA were stimulated with SIINFEKL peptide (0.5 μ g/ml). For adoptive transfer of activated T-cells, splenocytes from OT-1 WT and SA were stimulated with SIINFEKL (0.5 μ g/ml) peptide in presence of human IL2 (50 IU/ml). After 2 days, cells were washed and split into new medium supplemented with IL2. Following 3 days of activation 2x10⁷ T cells were used for 4 consecutive daily i.v. injections.

Trans-well migration assay. Naive T cells from CD45.1 WT animals and CD45.2 SA animals were activated with plate bound anti-CD3 antibodies and soluble anti-CD28 antibodies for 2 days. Then cells were transferred to new plates and rested for additional 2 days. For trans-well migration assay cells were reconstituted in RPMI 1640/0.5% BSA (assay media) and transferred to upper chambers (100 μ l, 0.5x10⁶ cells) (insert). Inserts were then placed into 24 well plate filled with 600 μ l of assay media with different concentration of CXCL12 and CXCL9. Plate was placed in CO₂ incubator at 37°C. After 2 hr inserts were removed and transmigrated cells from the bottom chamber were spin down, manually count to determine the absolute number of migrated cells and stain with anti-CD3-APC/CD8-AF700/CD4-APC-Cy7/CD45.1-PE/CD45.1-FITC antibody cocktail and DAPI.

Analysis of antigen presentation and cross-presentation. CD11c⁺ dendritic cells were isolated from mouse spleens with CD11c MicroBeads (Miltenyi Biotec) and incubated with the OVA257-264 peptide (SIINFEKL; AnaSpec), or control human papillomavirus E7 protein (49-57) peptide (RAHYNIVTF; AnaSpec) for 1 hr at 37°C in (RPMI supplemented with 100 U/ml penicillin, 100 μ g/ml streptomycin, 10% FBS, 50 μ M 2- β ME, and 2 mM L-glutamine (complete medium). The cells were further washed three times with DPBS, re-suspended in complete medium and plated at 2x10⁴ cells/well in 96-well round-bottom plates (Corning) containing 2x10⁵ CFSE-labeled OT-1 cells. Proliferation of T cells was analyzed by flow cytometry after 2.5 days of culture. To evaluate antigen cross-presentation 2.5x10⁷ splenocytes from C3H/Hej mice were incubated in 170 μ l of hypertonic

medium (0.5 M sucrose, 10% wt/vol polyethylene glycol 1000, and 10 mM Hepes in RPMI 1640, pH 7.2) alone or in the presence of 10 mg/ml ovalbumin (Calbiochem) for 10 min at 37°C. 2.2 ml of pre-warmed hypotonic medium (40% H₂O, 60% RPMI 1640) was added followed by an additional 2 min incubation at 37°C. The cells were centrifuged, washed twice with cold PBS and irradiated (1,350 rads). For all cultures, 5x10⁴ irradiated ovalbumin loaded CD45.2⁺ C3H/Hej splenocytes were incubated in a round bottom 96-well plate (final volume: 200µl) with 5x10⁴ CFSE labeled CD45.1⁺ OT-1 transgenic T cells and 5x10⁴ splenic CD45.2⁺CD11c⁺ DCs from SA and WT mice in the presence of GM-CSF (150 IU/ml). As a positive control, 5x10⁴ CFSE labeled CD45.1⁺ OT-1 transgenic T cells and 5x10⁴ splenic CD45.2⁺CD11c⁺ cells from WT or SA mice were cultured in the continuous presence of 1 µM SIINFEKL (Ova 257-264) peptide. After 72 hr, cells were stained for CD45.1-APC and CD8-APC-Cy-7 and percentages of CD45.1⁺CD8⁺CFSE^{low} cells were assessed by flow.

To estimate antigen presentation in vivo naive IFNAR1^{WT} T cells were isolated from the spleens of OT-1 CD45.1 mice, labeled with CFSE and injected into SA and WT mice through the retro-orbital sinus (each mouse received 2.5x10⁶ cells). Next day mice were s.c. injected with MC38OVA cells (1x10⁶ cells) into the right flank. After 6 days spleens were isolated and the percentage and proliferation of CD45.1⁺CD45.2⁻CD8⁺ cells were quantified.

To analyze the antigen cross presentation by intra-tumoral DCs, *Rag1*^{-/-} WT and *Rag1*^{-/-} SA mice were subcutaneously injected with 2x10⁶ MC38-OVA^{bright} cells (100 µl). Tumors were harvested (at size ~100 mm²) and digested. The levels of OVA peptide (SIINFEKL)-H2Kb complex on the surface of CD45⁺CD11c⁺MHCII⁺CD103⁺ cells were assessed by flow cytometry using the 25-D1.16 monoclonal antibody (as described in (Baghdadi et al., 2013)).

Generation of mouse anti-FAP-CARs, retrovirus production and T cell transduction. The CAR migR1-Mu-FAP-CAR-GFP-JS construct used in this study was previously described (Wang et al., 2014). The mouse FAP-specific scFv used for generating the anti-FAP-CAR was derived from the FAP antibody (Wang et al., 2014). Retroviral supernatants were generated by co-transfected Phoenix cells (5x10⁶ cells plated on 100 mm plate 1 day before transfection) with the migR1-Mu-FAP-CAR-GFP-JS plasmid (18 µg/plate) and pCI-Eco packaging plasmid (9 µg/plate) the appropriate using Lipofectamine reagent 2000 (Invitrogen). Retroviral supernatants were collected at 48 hours after transfection, passed through 0.45 µm nylon filter, mixed with Polybrene (5 µg/ml, Santa Cruz Biotech) and transferred to 24-well plates. Activated T cells (2x10⁶ per well, at 2x10⁶ cells/ml in complete media supplemented with human IL2 (100 U/ml, eBioscience)) were then spun onto the retrovirus plates for 60 min at 1,300 g. Activated T cells were transduced overnight, then a half of the supernatant was removed from the plates and fresh media (1.5 ml/well) were added to each well. Cells were expanded for 3-4 days and adoptively transferred by retro-orbital injection into venous plexus of anesthetized tumor-bearing mice when tumors were typically 30-50 mm². The adoptively transferred T cells demonstrated >50% transduction efficiency determined by GFP expression.

To generate activated mouse T cells for transduction, purified T-cells (5x10⁶ per well, at 2.5x10⁶ cells/ml in IL2 containing T cell media) were activated for 48 hours in 12-well plates pre-coated with anti-CD3e (1 µg/well) and CD28 (2 µg/well) antibodies. To ablate p38α expression FAP-CAR T cells were generated from mice of the following genotypes: *Ifnar1*^{+/+} *Mapk14*^{f/f} (*Mapk14*^{f/f}, WT); Ubc-Cre^{ERT2} *Ifnar1*^{+/+} *Mapk14*^{f/f} (*Mapk14*^{ΔΔ}, WT); *Ifnar1*^{-/-} *Mapk14*^{f/f} (*Mapk14*^{f/f}, Null); and Ubc-Cre^{ERT2} *Ifnar1*^{-/-} *Mapk14*^{f/f} (*Mapk14*^{ΔΔ}, Null). These FAP-CAR T cells were treated for 24h with 1 µg/ml of 4-hydroxytamoxifen (Sigma) one day before adoptive transfer.

SUPPLEMENTAL REFERENCES

- Agesen, T. H., Sveen, A., Merok, M. A., Lind, G. E., Nesbakken, A., Skotheim, R. I., and Lothe, R. A. (2012). ColoGuideEx: a robust gene classifier specific for stage II colorectal cancer prognosis. *Gut* 61, 1560-1567.
- Baghdadi, M., Yoneda, A., Yamashina, T., Nagao, H., Komohara, Y., Nagai, S., Akiba, H., Foretz, M., Yoshiyama, H., Kinoshita, I., et al. (2013). TIM-4 glycoprotein-mediated degradation of dying tumor cells by autophagy leads to reduced antigen presentation and increased immune tolerance. *Immunity* 39, 1070-1081.
- Camp, R. L., Dolled-Filhart, M., and Rimm, D. L. (2004). X-tile: a new bio-informatics tool for biomarker assessment and outcome-based cut-point optimization. *Clin Cancer Res* 10, 7252-7259.
- Gilfillan, S., Chan, C. J., Cella, M., Haynes, N. M., Rapaport, A. S., Boles, K. S., Andrews, D. M., Smyth, M. J., and Colonna, M. (2008). DNAM-1 promotes activation of cytotoxic lymphocytes by nonprofessional antigen-presenting cells and tumors. *J Exp Med* 205, 2965-2973.
- Goswami, C. P., and Nakshatri, H. (2013). PROGgene: gene expression based survival analysis web application for multiple cancers. *J Clin Bioinforma* 3, 22.
- King, C. E., Cuatrecasas, M., Castells, A., Sepulveda, A. R., Lee, J. S., and Rustgi, A. K. (2011). LIN28B promotes colon cancer progression and metastasis. *Cancer Res* 71, 4260-4268.
- LeBaron, M. J., Crismon, H. R., Utama, F. E., Neilson, L. M., Sultan, A. S., Johnson, K. J., Andersson, E. C., and Rui, H. (2005). Ultrahigh density microarrays of solid samples. *Nat Methods* 2, 511-513.
- Peck, A. R., Girondo, M. A., Liu, C., Kovatich, A. J., Hooke, J. A., Shriver, C. D., Hu, H., Mitchell, E. P., Freydin, B., Hyslop, T., et al. (2016). Validation of tumor protein marker quantification by two independent automated immunofluorescence image analysis platforms. *Mod Pathol*.
- Peck, A. R., Witkiewicz, A. K., Liu, C., Stringer, G. A., Klimowicz, A. C., Pequignot, E., Freydin, B., Tran, T. H., Yang, N., Rosenberg, A. L., et al. (2011). Loss of nuclear localized and tyrosine phosphorylated Stat5 in breast cancer predicts poor clinical outcome and increased risk of antiestrogen therapy failure. *J Clin Oncol* 29, 2448-2458.
- Powell, A. E., Anderson, E. C., Davies, P. S., Silk, A. D., Pelz, C., Impey, S., and Wong, M. H. (2011). Fusion between Intestinal epithelial cells and macrophages in a cancer context results in nuclear reprogramming. *Cancer Res* 71, 1497-1505.
- Ramakrishnan, R., Tyurin, V. A., Veglia, F., Condamine, T., Amoscato, A., Mohammadyani, D., Johnson, J. J., Zhang, L. M., Klein-Seetharaman, J., Celis, E., et al. (2014). Oxidized lipids block antigen cross-presentation by dendritic cells in cancer. *J Immunol* 192, 2920-2931.
- Sheffer, M., Bacolod, M. D., Zuk, O., Giardina, S. F., Pincas, H., Barany, F., Paty, P. B., Gerald, W. L., Notterman, D. A., and Domany, E. (2009). Association of survival and disease progression with chromosomal instability: a genomic exploration of colorectal cancer. *Proc Natl Acad Sci U S A* 106, 7131-7136.
- Wilson, C., Lin, J. E., Li, P., Snook, A. E., Gong, J., Sato, T., Liu, C., Girondo, M. A., Rui, H., Hyslop, T., and Waldman, S. A. (2014). The paracrine hormone for the GUCY2C tumor suppressor, guanylin, is universally lost in colorectal cancer. *Cancer Epidemiol Biomarkers Prev* 23, 2328-2337.